Benchmarking time-dependent density functional theory for singlet excited states of thermally activated delayed fluorescence chromophores

Xiaopeng Wang [*]

*Qingdao Institute for Theoretical and Computational Sciences, Institute of Frontier and
Interdisciplinary Science, Shandong University, Qingdao, Shandong 266237, China*

Siyu Gao

Department of Materials Science and Engineering, Carnegie Mellon University, Pittsburgh, Pennsylvania 15213, USA

Mingwen Zhao

School of Physics and State Key Laboratory of Crystal Materials, Shandong University, Jinan, Shandong 250100, China

Noa Marom

*Department of Materials Science and Engineering, Carnegie Mellon University, Pittsburgh, Pennsylvania 15213, USA;
Department of Physics, Carnegie Mellon University, Pittsburgh, Pennsylvania 15213, USA;
and Department of Chemistry, Carnegie Mellon University, Pittsburgh, Pennsylvania 15213, USA*

Thermally activated delayed fluorescence (TADF) is the internal conversion of triplet excitons into singlet excitons via reverse intersystem crossing. TADF can significantly enhance the efficiency of organic light-emitting diodes (OLEDs). In order for a chromophore to display TADF the energy difference between its lowest singlet and lowest triplet states, S_1 and T_1, should be as small as possible. This requirement is facilitated by spatial separation between the frontier orbitals. Computer simulations based on time-dependent density functional theory (TDDFT) have been used extensively to predict the excited state properties of TADF chromophores. However, the accuracy of TDDFT largely depends on the choice of exchange-correlation functional. Here, we present a benchmark study of the performance of TDDFT based on different classes of hybrid functionals for 16 TADF chromophores consisting of different donor and acceptor moieties. We find that only the range-separated double hybrid functionals, ωB2PLYP and ωB2GP-PLYP, provide qualitatively correct predictions of the relative singlet excitation energies of different molecules, the spectral composition of excited states, and the energy ordering of intramolecular charge-transfer versus valence excited states. Therefore, we recommend using these functionals to assess prospective TADF chromophores. Nevertheless, further development is needed to improve the quantitative performance of TDDFT. These findings are important for our ability to computationally screen and design candidate TADF chromophores and advance the development of highly efficient OLEDs.

I. INTRODUCTION

Organic chromophores are widely used in organic electronic and photovoltaic devices [1,2], such as organic light-emitting diodes (OLEDs) [3,4]. The efficiency of OLEDs is limited because 75% of electrically generated excitons are triplet excitons [5], whose radiative decay to the singlet ground state is forbidden by selection rules. This loss may be mitigated by thermally activated delayed fluorescence (TADF) [5–13], a reverse intersystem crossing (RISC) from the lowest

triplet excited state T_1, to the lowest singlet excited state S_1, which subsequently decays to the ground state S_0, emitting a photon. TADF chromophores are organic molecules [5,6,14], metal-organic complexes [15–17], and polymers [18]. In addition to OLEDs, TADF chromophores can also be used as triplet sensitizers in triplet-triplet annihilation (TTA) upconversion thanks to the small energy difference between their S_1 and T_1 states, ΔE_{ST} [19–21].

The endothermic RISC process is thermally activated with an energy barrier of $\Delta E_{ST} = S_1 - T_1$. Therefore, strong emission was initially observed at elevated temperatures. The first reported pure organic TADF chromophore was eosin in 1961 with a ΔE_{ST} of 0.37 eV [11]. A breakthrough was achieved by Adachi *et al.*, who demonstrated that spatially separating the highest occupied molecular orbital (HOMO) and the lowest unoccupied molecular orbital (LUMO) leads to a small ΔE_{ST}, producing efficient TADF [12]. This can be explained within a simple two-electron two-state model [22], where ΔE_{ST}

---

[*]xiaopengwang@sdu.edu.cn

corresponds to twice the electron exchange energy, J. J depends on the spatial overlap between the two states. The smaller this spatial overlap, the smaller J is. Using this design approach, Adachi *et al.* synthesized a donor-acceptor molecule with ΔE_{ST} as small as 0.11 eV, showing both efficient upconversion from T_1 to S_1 and intense fluorescence. This has spurred research on TADF in the last decade, including experimental synthesis of new TADF chromophores [23–28], as well as theoretical studies of molecular properties [29–32], and/or molecular design principles [9,23–26,30,33–35].

Excitation energies of chromophores may be calculated accurately using high-level quantum chemistry methods, such as the spin-component scaling modification of the approximate coupled-cluster singles-and-doubles (SCS-CC2) [30,36,37] and the domain-based local pair natural orbital (DLPNO) implementation [38,39] of the similarity transformed equation of motion coupled cluster theory with single and double excitations (STEOM-CCSD) [40]. However, the high computational cost of these methods is prohibitive for materials screening. Thanks to the appealing balance between accuracy and efficiency, computer simulations based on density functional theory (DFT) and time-dependent DFT (TDDFT) [41,42] are widely used for the design of TADF chromophores by predicting the frontier molecular orbitals and excited state properties. Using TDDFT for high-throughput screening, thousands of molecules out of a set of 400 000 have been identified as promising TADF-based OLED chromophores across the visible spectrum and selected candidates have been experimentally determined to yield external quantum efficiencies as high as 22% [43]. TDDFT has been used to derive design principles for TADF chromophores. Using TDDFT, it has been demonstrated that a linker added between the donor and acceptor moieties, especially a nonaromatic linker, reduces the overlap between frontier orbitals, decreasing the exchange energy and ΔE_{ST} [29].

Despite the recent successes of TDDFT in deriving design rules for TADF chromophores, predicting the properties of putative molecules, and discovering new materials, its predictive power strongly depends on the choice of approximation for the exchange-correlation (xc) functional. The self-interaction error (SIE) affects the DFT orbital energies, in particular for semilocal functionals, typically leading to severely underestimated HOMO-LUMO gaps and destabilization of localized molecular orbitals [44–47]. SIEs in the ground-state orbital energies propagate to the TDDFT excited-state energies. In particular, SIE may cause drastic underestimation of the energies of charge-transfer (CT) excited states [48,49], where the electron and hole are spatially separated, such as the excitation from HOMO to LUMO in donor-acceptor molecules. Spurious CT states may be present in TDDFT spectra [50,51]. For donor-acceptor compounds, the energy of a CT excitation may be underestimated to the point that it becomes lower than non-CT (valence) excitations, leading to misidentification of the transitions contributing to S_1 and T_1. In global hybrid functionals the effect of SIE is mitigated by mixing a fraction of exact (Fock) exchange with the semi-local exchange and correlation. However, the large percentage of Fock exchange required to accurately describe CT states is detrimental to the overall accuracy [44]. In range-separated hybrid functionals

the Coulomb interaction is split into a short-range and a long-range component [52,53]. Long-range corrected (LC) hybrid functionals contain a larger fraction of Fock exchange in the long range and a reduced fraction of Fock exchange in the short range [54–58]. This provides an improved description of CT excitations [59–61]. The fraction of Fock exchange included in the short range and the range-separation parameter of LC-hybrid functionals may be tuned to system-specific values, which may further improve the performance for a given system [62–64].

TADF chromophores often incorporate a twisted torsion angle or a linker between the donor and acceptor moieties to facilitate the spatial localization and separation of the HOMO and LUMO [5]. Visualization of DFT orbitals has been used in studies of new experimentally synthesized and theoretically predicted TADF candidates to assess the degree of orbital localization and separation [5,65]. However, visual inspection of DFT orbitals does not guarantee that the S_1 and T_1 excited states will be dominated by a CT-like transition between the spatially separated HOMO and LUMO. To calculate the energies and spectral composition of S_1 and T_1 in TADF chromophores, TDDFT has been widely used [6], predominantly with the Becke 3-parameter Lee-Yang-Parr (B3LYP) [66] and the Perdew-Burke-Ernzerhof based (PBE0) [67] global hybrid functionals [17,25,68–79]. Fewer studies of TADF chromophores have utilized other functionals [6,22,80–82], including the Minnesota global hybrid meta generalized gradient approximation (meta-GGA) with double Fock exchange (M06-2X) [83], the range-separated Coulomb-attenuating method B3LYP functional (CAM-B3LYP) [54], and the range-separated hybrid functionals ωB97X [56] and ωB97X-D [84]. In some cases, findings obtained with a global hybrid functional may not hold with a LC-hybrid functional. For example, TDDFT with global hybrid functionals may underestimate CT excitation energies, overestimating the CT character of S_1 and T_1 and incorrectly predicting an effective TADF chromophore [27,48,49,85]. Therefore, a benchmark study of the performance of TDDFT for intramolecular CT states using different functionals is important for our ability to reliably predict the properties of proposed TADF chromophores and advance the development of highly efficient OLEDs.

Several studies have benchmarked the performance of TDDFT using different functionals, with respect to experimental values and high-level calculations of the excitation energies of various molecules [86–91]. Some studies have focused specifically on CT excited states [92–98] and TADF chromophores [13,27,28,32,99–102]. The latter studies have used experimental values of the excitation energies of known TADF chromophores as the performance metrics. One drawback of this approach is that for these chromophores the experimental observation of TADF already indicates that the lowest excitations are dominated by a CT-like transition from HOMO to LUMO. Therefore, the S_1 energies of such molecules are not useful for assessing whether different functionals underestimate the CT excitation to be lower than valence excitations, leading to a qualitatively incorrect lowest excited state. Rather, a donor-acceptor molecule with a valence lowest excited state should be used for this purpose.

As a case study, we have chosen a donor-acceptor molecule consisting of a carbazole donor and a cyanobenzene acceptor (CzCB). As we demonstrate below, at any torsion angle between the donor and acceptor moieties S_1 is dominated by valence transitions and remains a valence excited state. We use this to evaluate whether TDDFT with different functionals erroneously predicts a CT-like S_1 excitation. In addition, we have compiled a benchmark set of 15 molecules consisting of different donor and acceptor moieties commonly used in experiments to provide a statistical assessment of functional performance for a wider array of materials. In contrast to earlier benchmarks [13,27,28,32,99–102], which focused only on the excitation energies, we also evaluate the performance of TDDFT with respect to the spectral composition of the S_1 excitation, namely the contribution of the HOMO → LUMO transition. We benchmark five classes of functionals, including global hybrid functionals, global hybrid meta-GGA functionals, LC-hybrid functionals, perturbatively corrected double hybrid functionals, in which generalized gradient approximations are mixed with Fock exchange and a fractional correlation energy calculated at the level of second-order many-body perturbation theory (PT2), and range separated double hybrid functionals. In addition, we explore whether system-specific tuning improves the performance of LC-hybrid functionals. We note that only singlet intramolecular CT excitation energies are benchmarked due to the lack of experimental triplet excitation energies of the TADF benchmark set. Moreover, triplet excitation energies may be affected by triplet instability, which may be exacerbated by the inclusion of Fock exchange [103–105], requiring further benchmarks.

TDDFT results are compared to experimental values, where available, and to high-level theoretical values obtained using DLPNO-STEOM-CCSD. The equation of motion (EOM) approach is an extension of the ground-state coupled cluster (CC) theory to compute excitation energies by a linear operator on the similarity transformed Hamiltonian [106]. EOM-CCSD scales proportional to the sixth power of the system size. Nooijen *et al.* proposed STEOM-CCSD, where a second similarity transformation is performed to reduce the cost of evaluating the transformed equations and yield more accurate excitation energies than EOM-CCSD because STEOM-CCSD contains some triple excitation effects. The DLPNO technique [38,39], newly developed by Neese *et al.*, enables computing the ground state CC energies for large molecules. It has been shown that the DLPNO-STEOM-CCSD approach does not lose any significant accuracy relative to its canonical counterpart for benchmark sets such as Thiel's set [106–111]. The DLPNO version of EOM-CCSD has been found to produce an average absolute deviation of 0.042, 0.079, and 0.128 eV, respectively, for ionization energies from the HOMO, outer valence, and inner valence orbitals, which is on the order of the intrinsic error of the canonical version itself [107]. The DLPNO implementation has reproduced the electron affinities (EA) obtained with EOM-CCSD with a maximum absolute deviation of 49 meV for a test set of 24 molecules [108]. The DLPNO-STEOM-CCSD approach is employed to provide reliable information on the spectral composition of the excited states, which is

missing from benchmarks that rely only on comparison to experimental excitation energies.

We find that only LC-BLYP and ωB97X LC hybrid functionals, with 100% Fock exchange in the long range and a range separation parameter of about 0.3 bohr^{-1}, and the ωB2PLYP and ωB2GP-PLYP range-separated double hybrid functionals correctly capture the spectral composition of intramolecular CT states. Other functionals underestimate CT excitation energies and thus overestimate the contribution of CT transitions between spatially separated frontier orbitals to the lowest excited state. The LC-BLYP and ωB97X functionals may, in contrast, overestimate excitation energies of CT states to be erroneously higher than valence excited states. This leaves only the ωB2PLYP and ωB2GP-PLYP range-separated double hybrid functionals as the most reliable for predicting the excited states of TADF chromophores. New range separated double hybrid functionals may be explored to further improve the accuracy of the energy spacing between different states.

II. METHODS

A. Exchange-correlation functionals

TDDFT calculations were performed with several functionals of different classes. The lowest three rungs in the "Jacob's ladder" of density functional approximations [112], namely the local density approximation (LDA), generalized gradient approximation (GGA), and meta-GGA, are not considered here. Rather, we start from "fourth rung" hybrid GGA and hybrid meta-GGA functionals with inclusion of Fock exchange. As summarized in Table I, the B3LYP [66] and PBE0 [67] global hybrid GGA functionals contain a fixed fraction of Fock exchange mixed with GGA exchange and correlation. The B3LYP functional

TABLE I. Percentage of exact (Fock) exchange (EXX) for global hybrid GGA, meta-GGA, and double hybrid functionals, EXX^G, percentage of Fock exchange in the short range, EXX^{SR}, and long range, EXX^{LR}, and range separation parameter, ω, for range-separated hybrid and double hybrid functionals, and percentage of PT2 correlation for double hybrid and range-separated double hybrid functionals. The unit of ω is bohr^{-1}.

	EXX^G	EXX^{SR}	EXX^{LR}	ω	PT2
B3LYP [66]	20%				
PBE0 [67]	25%				
TPSSh [113]	10%				
M06-2X [83]	54%				
CAM-B3LYP [54]		19%	65%	0.33	
LC-BLYP [55]		0%	100%	0.33	
ωB97X [56]		15.7706%	100%	0.30	
IP-LC-BLYP		0%	100%	tuned[a]	
IP-ωB97X		15.7706%	100%	tuned[a]	
B2PLYP [114]	53%				27%
B2GP-PLYP [115]	65%				36%
ωB2PLYP [116]		53%	100%	0.30	27%
ωB2GP-PLYP [116]		65%	100%	0.27	36%

[a]Tuned system-specific value.

contains 20% Fock exchange mixed with the Becke semilocal exchange and the Vosko-Wilk-Nusair (VWN) local correlation and the Lee-Yang-Parr (LYP) correlation, whereas the PBE0 functional contains 25% Fock exchange mixed with the Perdew-Burke-Ernzerhof exchange and correlation. The global hybrid meta-GGA functionals of Tao-Perdew-Staroverov-Scuseria (TPSSh) [113] and M06-2X [83] contain a fixed fraction of Fock exchange mixed with meta-GGA exchange and correlation. Meta-GGA functionals contain a dependence on the kinetic energy density in addition to the density and its gradient. TPSSh contains 10% Fock exchange and nonempirical Tao-Perdew-Staroverov-Scuseria (TPSS) meta-GGA, whereas the semi-empirical M06-2X with 54% Fock exchange is heavily-parameterized for nonmetals and is recommended for applications involving excitation energies of valence and Rydberg states [83].

In the global double hybrid functional B2PLYP [114] and B2GP-PLYP [115], the GGA Becke exchange and LYP correlation are mixed with Fock exchange and perturbative second-order correlation (PT2) [117–119]. They are hence named double hybrid. Double hybrids are considered as "fifth rung" functionals because unoccupied Kohn-Sham orbitals are used for calculating the PT2 correlation energy [120,121]. The difference between B2PLYP and B2GP-PLYP is the mixing fractions obtained based on different fitting sets [114,115]. The former contains 53% Fock exchange and 27% PT2 correlation, whereas the latter contains 65% Fock exchange and 36% PT2 correlation.

In range-separated hybrid functionals the Coulomb interaction is split into short range (SR) and long range (LR) parts and the fraction of Fock exchange depends on the spatial distance between two points. In the CAM-B3LYP [54] functional, the fraction of Fock exchange increases from 19% in the short range to 65% in the long range. In the LC-BLYP [55] functional the fraction of Fock exchange varies from 0% to 100% and in the ωB97X [56] functional the fraction of Fock exchange ranges from 15.7706% to 100%. The intermediate region is usually smoothly described by the standard error function with a range separation parameter ω, which is typically determined by fitting empirically to a benchmark set. The range separation parameter is 0.33 bohr^{-1} in CAM-B3LYP, 0.33 bohr^{-1} in LC-BLYP, and 0.30 bohr^{-1} in ωB97X. CAM-B3LYP, LC-BLYP, and ωB97X are derived by modifying the exchange in B3LYP, BLYP [122], and B97 [123] functionals, respectively. CAM-B3LYP employs the same Becke exchange and VWN and LYP correlation as B3LYP. LC-BLYP uses the same Becke exchange and LYP correlation as in the BLYP GGA functional [122]. ωB97X uses exchange and correlation that are of the form suggested by Becke in his 1997 global hybrid GGA functional, B97.[123] In the same vein, Casanova-Paez *et al.* proposed the range-separated double hybrid functionals ωB2PLYP [116] and ωB2GP-PLYP [116] by introducing range separation to the exchange part of the double hybrid functionals B2PLYP and B2GP-PLYP,

$$E_{XC} = \alpha E_X^{\omega B88}(\omega) + (1 - \alpha)E_X^{SR-HF} + E_X^{LR-HF}$$
$$+ \beta E_C^{LYP} + (1 - \beta)E_C^{PT2}. \quad (1)$$

The α and β parameters in ωB2PLYP and ωB2GP-PLYP are kept the same as in B2PLYP ($\alpha = 0.47$, $\beta = 0.73$) and
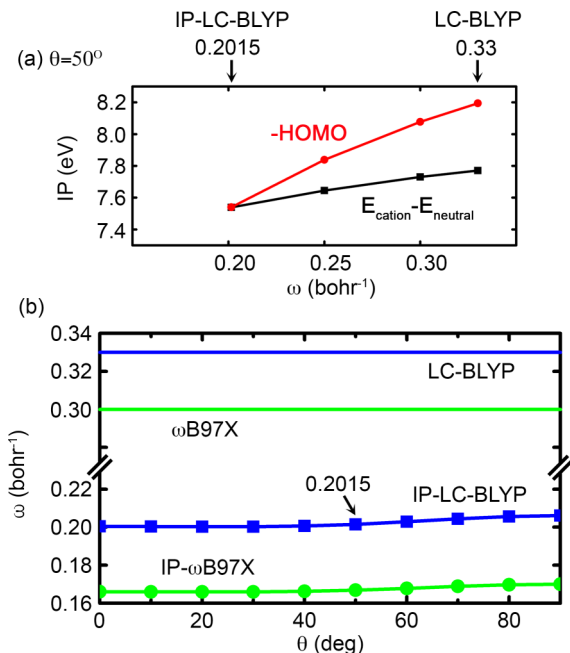

FIG. 1. (a) The IP of CzCB at the equilibrium dihedral angle of $\theta = 50°$, obtained from the negative of the HOMO energy (red) and the IP, given by the total energy difference between the cation and neutral molecules (black) as a function of the range separation parameter ω. (b) ω in LC-BLYP, ωB97X, IP-LC-BLYP, and IP-ωB97X as a function of the dihedral angle θ of CzCB.

B2GP-PLYP ($\alpha = 0.35$, $\beta = 0.64$), leaving only ω to be tuned. Casanova-Paez *et al.* tuned ω to reproduce the HOMO-LUMO gap by means of Koopmans theorem and to reduce the one-electron self-interaction error in the hydrogen atom. They found that, other than the aforementioned two nonempirical approaches, the most viable approach is an empirical least-squares fit to a training set consisting of Rydberg, CT, and local valence excited states, yielding ω values of 0.30 bohr^{-1} for ωB2PLYP and 0.27 bohr^{-1} for ωB2GP-PLYP [116]. These values are very close to 0.33 bohr^{-1} in CAM-B3LYP and LC-BLYP, and 0.30 bohr^{-1} in ωB97X. The ωB2PLYP and ωB2GP-PLYP functionals are thus tailored for TDDFT excited states rather than ground state properties.

Alternatively, ω may be tuned to a system-specific value, for example by reproducing the ionization potential (IP) of the molecule of interest by means of Koopmans' theorem [124]. In addition to the aforementioned 11 functionals, we considered system-specific nonempirically IP-tuned LC-BLYP and ωB97X, denoted as IP-LC-BLYP and IP-ωB97X. Figure 1(a) shows the IP-tuning procedure for CzCB at the equilibrium dihedral angle of $\theta = 50°$. To make the negative of the HOMO energy equal to the IP, given by the total energy difference between the cation and neutral molecules, ω is decreased from 0.33 bohr^{-1} in LC-BLYP to 0.2015 bohr^{-1} in IP-LC-BLYP. Figure 1(b) shows the IP-tuned ω in IP-LC-BLYP and IP-ωB97X as a function of the dihedral angle. For both functionals, IP-tuning produces ω values that are significantly lower than the constant ω values in LC-BLYP and ωB97X for all 10 molecular geometries. The IP-tuned ω values have a weak dependence on the molecular conformation.

B. Computational details

All calculations were conducted using version 4.2.0 of the ORCA code [125]. Geometry optimizations were performed using the B3LYP functional [66], and a pairwise dispersion correction with the Becke-Johnson damping [126]. SV(P) basis sets were used and tight SCF convergence criteria corresponding to an energy tolerance of 1×10^{-8} au were applied. All atomic positions were relaxed until the maximal force was below 3×10^{-4} au. For CzCB, the optimal dihedral angle between the carbazole and cyanobenzene planes, θ, was found to be $50°$. To modify the overlap of the HOMO and LUMO, θ was varied from $0°$ to $90°$ by increments of $10°$, with the atomic positions within the donor and acceptor moieties fixed. The 10 resulting molecular geometries of CzCB and the TADF benchmark set were used for DLPNO-STEOM-CCSD and TDDFT calculations.

Reference DLPNO-STEOM-CCSD calculations were performed using the def2-TZVP basis sets [127], which provide a balance between accuracy and efficiency. For example, the agreement between DLPNO-STEOM-CCSD results obtained with def2-TZVP basis sets and experimental excitation energies of indigo dyes has been reported to be well below 0.1 eV [110,128]. The mean absolute error of values obtained with def2-TZVP compared to def2-QZVPP has been found to be only 0.01 eV [128]. The resolution of identity (RI) approximation was used with the def2-TZVP/C auxiliary basis sets [129]. The truncation parameter for singles pair natural orbitals (PNOs) was 1×10^{-11}, and the active space selection thresholds for occupied and virtual orbitals were set to 5×10^{-3} [108].

TDDFT calculations were performed using the def2-TZVP basis sets [127]. We have conducted a basis set convergence test for a representative TDDFT@B3LYP calculation of CzCB, provided in the SI. The energy difference between the values of the lowest four excitation energies obtained with def2-TZVP and def2-QZVPP is within 0.02 eV. The resolution of the identity (RI) approximation for the Møller-Plesset perturbation theory (MP2) was utilized with def2-TZVP/C auxiliary basis set [129] in the TDDFT calculations with double hybrid and range-separated double hybrid functionals.

Bader analysis [130,131] is a widely-used spatial partitioning scheme applied to charge densities in the format of volumetric data on a discrete three-dimensional grid. It was employed to calculate the charge distribution of molecular orbitals and evaluate the electron density differences between excited and ground states. The densities of molecular orbitals were computed with the FHI-aims code [132,133] using tier 2 basis sets [134] and output in the format of $100 \times 100 \times 100$ voxel grids in a $30 \times 30 \times 30$ bohr^3 cell. The electron density differences between excited states and ground states were computed with TDDFT using ORCA and output in the format of $80 \times 80 \times 80$ grids in a $28 \times 30 \times 31$ bohr^3 cell.

III. RESULTS AND DISCUSSION

A. A case study of CzCB

Figure 2(a) shows the change in the energies and spatial distributions of the Hartree-Fock orbitals of CzCB, which serve as the reference ground state for coupled cluster calculations, as a function of the dihedral angle, θ. The HOMO-1 and LUMO + 2 are localized on either the donor or the acceptor moiety regardless of the dihedral angle, whereas the HOMO-3, HOMO-2, HOMO, LUMO, and LUMO + 1 have a strong dependence on the molecular conformation. At $\theta = 0°$, the HOMO-3, HOMO-2, HOMO, LUMO, and LUMO + 1 extend over the whole molecule. As θ increases, the coupling between the π electron systems of the two moieties is broken. The HOMO-3, HOMO, and LUMO + 1 gradually become localized over the donor moiety and the HOMO-2 and LUMO gradually become localized over the acceptor moiety. As a result of the change in orbital localization, transitions involving these orbitals may exhibit a change of character upon bond rotation. In particular, the HOMO to LUMO transition changes from a valence excitation at $\theta = 0°$ to a CT-like excitation between the carbazole and the cyanobenzene at $\theta = 90°$. In addition to the qualitative visual inspection of molecular orbitals, this change in the character of the HOMO $\rightarrow$ LUMO transition may be quantified by Bader charge analysis. The percentage of charge on the acceptor moiety $\%e^A$ for the HOMO and LUMO is shown in Fig. 2(b). At $\theta = 0°$, the HOMO and LUMO are delocalized over the whole molecule and the charge population on the acceptor moiety is approximately equal, implying a valence transition from HOMO to LUMO. When θ approaches $90°$, the HOMO and LUMO are almost 100% localized over the donor and acceptor moieties, respectively, implying a CT transition. We note that DFT orbitals obtained with all functionals studied here reproduce the spatial distributions obtained with Hartree-Fock, however the orbital energies are different. Representative orbitals of DFT@B3LYP are visualized in the Supplemental Material [135]. The change of energy ordering between the HOMO-1 and HOMO, seen in Fig. 2, is not observed in DFT with any functional. Rather, a change of energy ordering between LUMO + 1 and LUMO + 2 at $50° < \theta < 90°$ is found in the DFT orbitals obtained with the B3LYP, PBE0, TPSSh, IP-LC-BLYP, and IP-ωB97X functionals. DFT orbital energies obtained with different functionals are provided in the Supplemental Material [135].

We begin by analyzing the dependence of the S_1 energy and spectral composition on the dihedral angle with DLPNO-STEOM-CCSD. Figure 3(a) shows that the DLPNO-STEOM-CCSD S_1 energy increases as θ is rotated from 0 to $90°$. Figure 3(b) shows the main transitions that contribute to S_1 as a function of θ. At $\theta = 0°$, S_1 is dominated by the transition from HOMO to LUMO. As θ increases, the HOMO to LUMO transition gradually changes from a valence excitation to a CT-like excitation, as the HOMO becomes localized on the donor moiety and the LUMO becomes localized on the acceptor moiety (see Fig. 2). The diminishing spatial overlap between the HOMO and LUMO leads to a decrease in the contribution of the HOMO $\rightarrow$ LUMO transition to S_1. At the same time, as θ increases, the LUMO + 1 becomes increasingly localized on the donor moiety (see Fig. 2). The HOMO and LUMO + 1 retain spatial overlap, leading to an increase in the contribution of the HOMO $\rightarrow$ LUMO + 1 transition to S_1. Overall, as its spectral composition changes, the S_1 excitation retains its valence character and does not become a CT-like excitation. This adversely affects the TADF performance of CzCB.
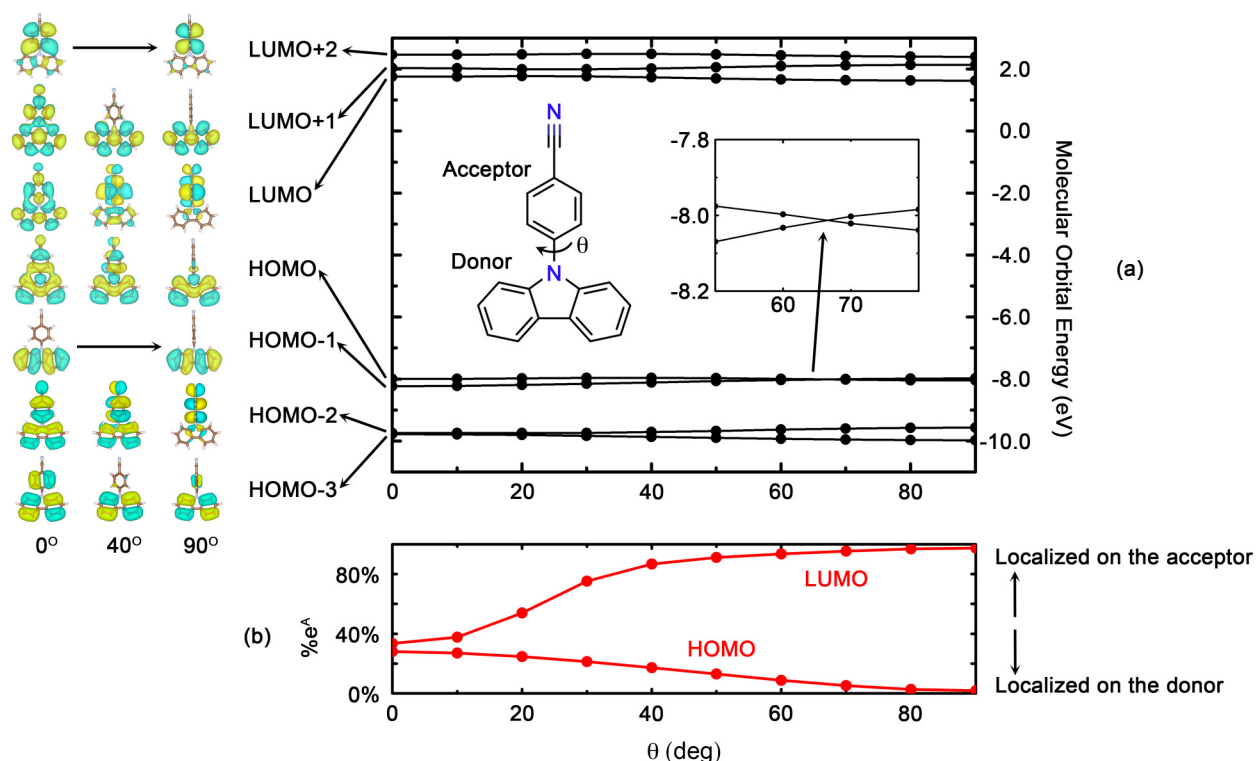
FIG. 2. (a) Molecular orbitals (HOMO-3 to LUMO + 2) and orbital energies of CzCB obtained with Hartree-Fock. The orbitals are labeled according to their energy ordering at the equilibrium torsion angle of $50°$. Orbitals are visualized with an isosurface value of 0.013 au. The inset shows the crossing of HOMO and HOMO-1 between $60°$ and $70°$. (b) Percentage of charge localized on the acceptor moiety for the HOMO and LUMO $\%e^A$ obtained with Bader analysis.
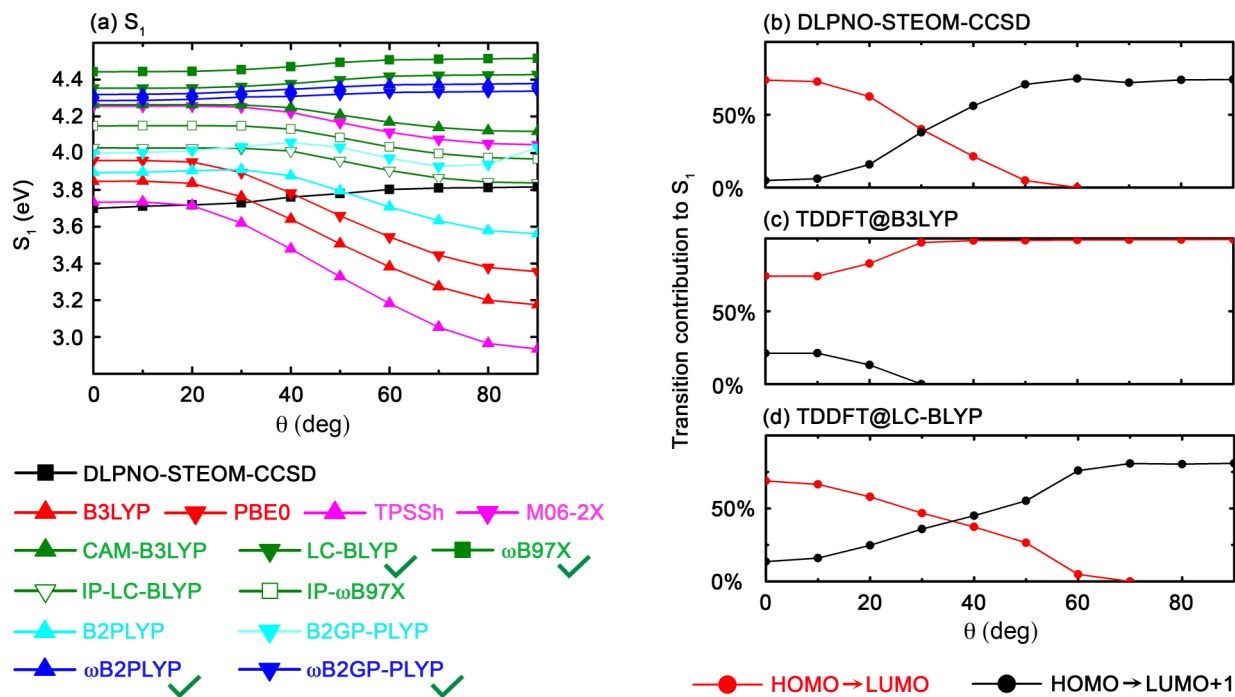

FIG. 3. (a) DLPNO-STEOM-CCSD and TDDFT S_1 energies as a function of θ. Check marks indicate that the correct qualitative behavior obtained with DLPNO-STEOM-CCSD is reproduced with TDDFT. The spectral composition of S_1 calculated with (b) DLPNO-STEOM-CCSD, (c) TDDFT@B3LYP, and (d) TDDFT@LC-BLYP.

We now turn to investigating whether TDDFT with different exchange-correlation functionals provides a qualitatively correct picture of the nature of the S_1 excitation of CzCB, which is crucial for reliably assessing its TADF performance. Figure 3(a) shows that only the LC-BLYP and ωB97X range-separated hybrid functionals and the ωB2PLYP and ωB2GP-PLYP range-separated double hybrid functionals reproduce the qualitative trend in S_1 versus θ obtained with DLPNO-STEOM-CCSD. With other functionals, the S_1 energy decreases rather than increases with θ. An analysis of the transitions contributing to S_1 explains why. Figure 3(c) shows that with TDDFT@B3LYP the contribution of the HOMO $\rightarrow$ LUMO transition to S_1 increases with θ rather than decreases, whereas the contribution of the HOMO $\rightarrow$ LUMO + 1 transition to S_1 decreases rather than increases. This means that above $\theta = 10°$ TDDFT@B3LYP erroneously predicts S_1 to be a CT excitation. Similar trends to B3LYP in the spectral composition of S_1 are obtained using the PBE0, TPSSh, M06-2X, CAM-B3LYP, IP-LC-BLYP, IP-ωB97X, B2PLYP, and B2GP-PLYP functionals, as shown in the Supplemental Material [135]. In contrast, TDDFT@LC-BLYP, shown in Fig. 3(d), reproduces the trends obtained with DLPNO-STEOM-CCSD. The contribution of the HOMO $\rightarrow$ LUMO transition to S_1 decreases with θ, whereas the contribution of the HOMO $\rightarrow$ LUMO + 1 transition increases, such that S_1 has a valence excitation character. Similar trends are obtained using the ωB97X, ωB2PLYP, and ωB2GP-PLYP functionals, as shown in the Supplemental Material [135]. The S_1 energy obtained with LC-BLYP, ωB97X, ωB2PLYP, and ωB2GP-PLYP increases with θ because the CT HOMO $\rightarrow$ LUMO transition is replaced by a valence transition from the HOMO to the higher-energy LUMO + 1. In contrast, with other functionals the S_1 energy decreases because the energy of the CT HOMO $\rightarrow$ LUMO transition is underestimated and it remains the dominant contribution to S_1.

This is further illustrated by the CT character of the S_1 excited state, CT^{DA}, plotted as a function of θ in Fig. 4. We define CT^{DA} as the amount of charge transferred from the donor moiety to the acceptor moiety, which corresponds to the electron density difference between the S_1 excited state and the S_0 ground state, $\Delta\rho$, over the acceptor moiety,

$$CT^{DA} = \int_A \Delta\rho \, dr^3. \qquad (2)$$

CT^{DA} is evaluated with Bader analysis. A positive value means net charge transfer from the donor (D) to the acceptor (A) moiety. The group of functionals that correctly describe the dependence of the S_1 energy on θ, LC-BLYP, ωB97X, ωB2PLYP, and ωB2GP-PLYP, show negligible charge transfer over the entire range of θ, which indicates a valence character. Although S_1 retains its valence character with bond rotation, its spatial distribution changes from an excitation delocalized over the whole molecule at $\theta = 0°$ to an excitation localized over the donor moiety at $\theta = 90°$. This is reflected in the electron density differences shown in Fig. 4. In contrast, the group of functionals that incorrectly describe the dependence of the S_1 energy on θ, B3LYP, PBE0, TPSSh, M06-2X, CAM-B3LYP, IP-LC-BLYP, IP-ωB97X, and B2PLYP, show electron transfer from the carbazole to the cyanobenzene, which becomes more significant at higher angles. With
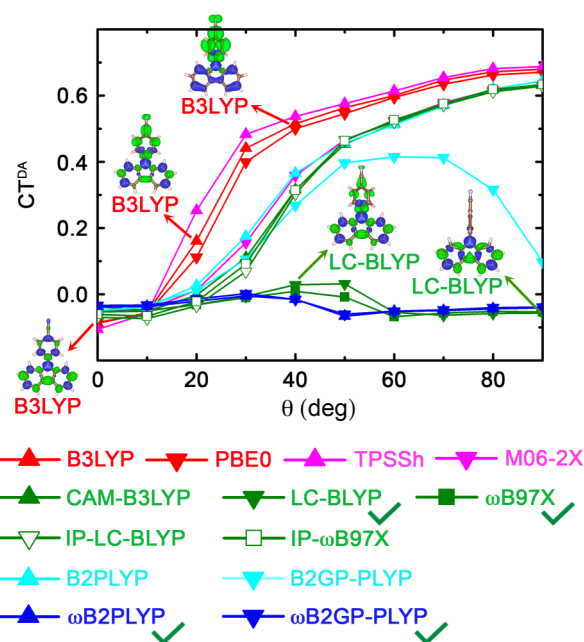

FIG. 4. CT^{DA}, computed with Bader analysis, as a function of θ. Check marks indicate that the correct qualitative behavior obtained with DLPNO-STEOM-CCSD is reproduced with TDDFT. Representative electron density differences, $\Delta\rho$, obtained with TDDFT@B3LYP and TDDFT@LC-BLYP are visualized with an isosurface value of 0.001 au. The green and blue represent positive $\Delta\rho$ (electron gain) and negative $\Delta\rho$ (electron loss).

B2GP-PLYP the electron transfer increases up to $\theta = 70°$ and subsequently decreases. This is because the energy of the CT HOMO $\rightarrow$ LUMO excitation is underestimated to be lower than, but very close to, the valence HOMO $\rightarrow$ LUMO + 1 excitation with TDDFT@B2GP-PLYP, as shown in the Supplemental Material [135].

The success of the LC-BLYP, ωB97X, ωB2PLYP, and ωB2GP-PLYP functionals in correctly describing the nature of the first singlet excited state of CzCB and its behavior as a function of molecular conformation is attributed to the inclusion of 100% Fock exchange in the long range, which is known to be important for the description of CT excitations [136–138]. Conversely, the failure of the CAM-B3LYP range-separated hybrid functional may be attributed to the lower fraction of 65% Fock exchange in the long range. The failure of double hybrid functionals and success of range-separated double hybrid functionals in calculating CT excited states are consistent with previous benchmarks [13,85,116,139]. We note, however, that the functionals that achieve a balanced description of CT and valence excitations and provide a qualitatively correct picture do not produce quantitatively accurate excitation energies. TDDFT based on LC-BLYP, ωB97X, ωB2PLYP, and ωB2GP-PLYP significantly overestimates the S_1 energy of CzCB compared to the DLPNO-STEOM-CCSD reference values, agreeing with benchmarks of CT states in other molecules [93] and our TADF molecule set below.

Optimally tuned system-specific range-separation parameters often improve the performance of range-separated hybrid functionals [140–142]. However, in some cases they may lead to large errors and qualitatively incorrect ground-state
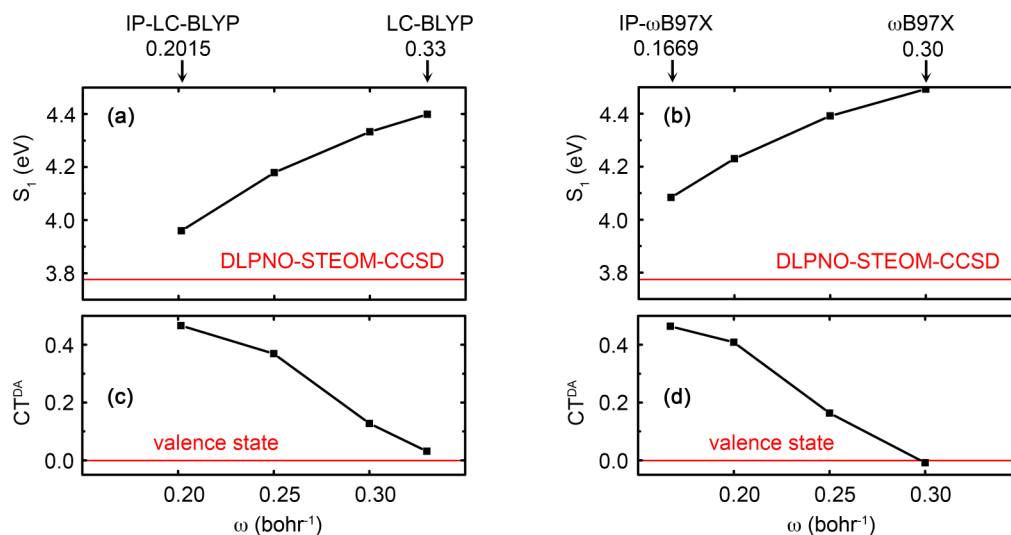
FIG. 5. [(a), (b)] TDDFT S_1 energy and [(c), (d)] CT^{DA} of the S_1 excitation of CzCB at the equilibrium conformation of $\theta = 50°$ as a function of the range separation parameter, ω, obtained with LC-BLYP and IP-LC-BLYP (left) and ωB97X and IP-ωB97X (right).

properties [143]. Figure 3(a) shows that the TDDFT@IP-LC-BLYP and TDDFT@IP-ωB97X S_1 energies are closer to the DLPNO-STEOM-CCSD reference than TDDFT@LC-BLYP and TDDFT@ωB97X. However, they erroneously decrease with θ. Figure 5 illustrates the changes in the energy and CT character of S_1 upon tuning ω from its values in LC-BLYP and ωB97X to IP-LC-BLYP and IP-ωB97X. For both functionals, the S_1 excitation energy decreases with ω and the character of S_1 changes from a valence to CT excited state. Therefore, system-specific IP-tuning does not improve the performance of the LC-BLYP and ωB97X range-separated hybrid functionals due to an underestimation of the CT HOMO $\rightarrow$ LUMO excitation energy. This is consistent with the failure of CAM-B3LYP because decreasing the range separation parameters reduces the amount of Fock exchange. Together with a 100% Fock exchange in the long range, a range separation parameter of at least $0.3\,\text{bohr}^{-1}$ in range-separated hybrid functionals is essential for a balanced description of valence and intramolecular CT excitations in CzCB. For a statistical performance evaluation of the LC-BLYP, ωB97X, ωB2PLYP, and ωB2GP-PLYP functionals, a set of 15 donor-acceptor molecules are calculated with DLPNO-STEOM-CCSD and TDDFT. The results are compared to experiments where available.

B. A TADF benchmark set

Figure 6 shows the structures of 15 TADF chromophores, denoted as **1** to **15**, consisting of different donor and acceptor moieties commonly used in experiments. The full chemical names are provided in the Supplemental Material [135]. Molecules **9** and **11** are theoretically proposed TADF candidates [144,145]. Others are experimentally synthesized compounds [28,65,71,146–155]. Their HOMO and LUMO are localized on the donor and acceptor moieties, as shown in the Supplemental Material [135], although, in some cases, the frontier orbitals may partially overlap. Computed S_1 energies may be compared with experimental measurements of the first absorption peaks. The degree of CT character is quantified

by the contribution of the HOMO $\rightarrow$ LUMO transition to the S_1 excitation, obtained with DLPNO-STEOM-CCSD, %HL. The benchmark set contains molecules whose S_1 excited states have different characters, as shown in Fig. 6. %HL is only 0.0% for **2** and 8.9% for **4**. For the remaining molecules, %HL ranges from 47.7% to 89.8%, indicating a significant CT character. Based on our findings for CzCB, TDDFT calculations for the TADF benchmark set are performed with the 7 range-separated hybrid and range-separated double hybrid functionals, i.e., CAM-B3LYP, LC-BLYP, ωB97X, IP-LC-BLYP, IP-ωB97X, ωB2PLYP, and ωB2GP-PLYP.

Figure 7(a) shows the difference between the S_1 energies calculated with TDDFT and the DLPNO-STEOM-CCSD reference values. The benchmark TADF chromophores are arranged by their %HL on the x axis. Comparison to experimental values, where available, is provided in the Supplemental Material [135]. The mean average errors (MAEs) of all methods are summarized in Fig. 7(b). Compared to experiments, DLPNO-STEOM-CCSD performs extremely well with a MAE of 0.09 eV, agreeing with previous benchmarks of other molecules [128]. For TDDFT calculations, the MAE has a strong dependence on the exchange-correlation functional, especially the fraction of Fock exchange. With LC-BLYP and ωB97X, the S_1 energy is significantly overestimated with MAEs of 0.66 and 0.78 eV. This agrees with the results reported here for CzCB, and with earlier benchmarks [93]. For CAM-B3LYP, IP-LC-BLYP, and IP-ωB97X, which contain less Fock exchange than LC-BLYP and ωB97X, the overestimation of the S_1 energy decreases with MAEs of 0.34, 0.16, and 0.17 eV. Notably, the performance of CAM-B3LYP, IP-LC-BLYP, and IP-ωB97X functionals depends on the nature of the excited state. For valence states, such as of molecules **2** and **4**, TDDFT S_1 excitation energies obtained with the CAM-B3LYP, IP-LC-BLYP, and IP-ωB97X functionals are overestimated by about 0.56, 0.27, and 0.41 eV with respect to the DLPNO-STEOM-CCSD reference in Fig. 7(a). For molecules **15** and **3** with %HL of 47.7% and 58.6%, respectively, the overestimation decreases by about 0.20 eV. For molecules whose S_1 has a
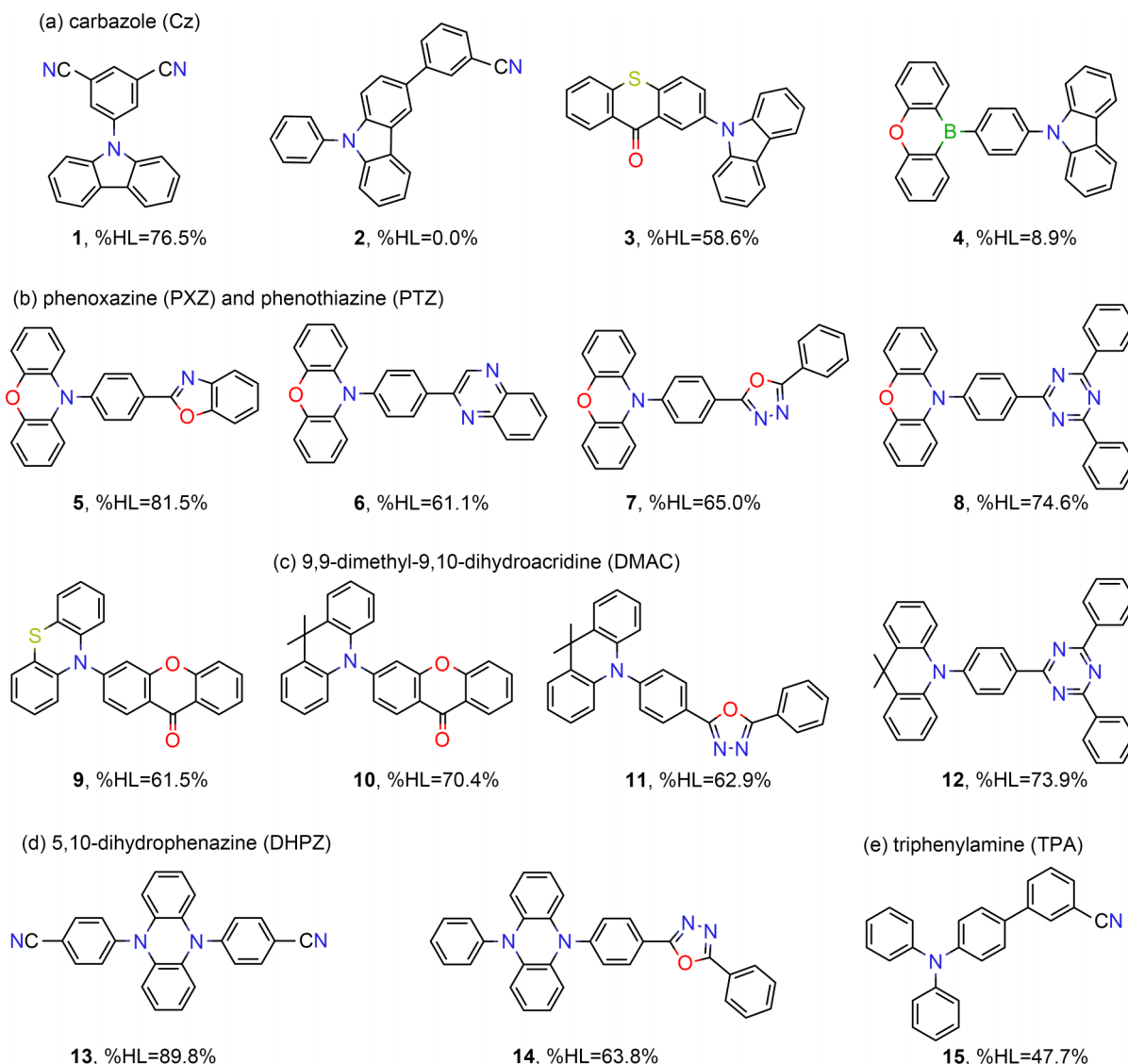
FIG. 6. Geometries of TADF chromophores, arranged by their donor moieties, i.e., (a) carbazole (Cz), (b) phenoxazine (PXZ) and phenothiazine (PTZ), (c) 9,9-dimethyl-9,10-dihydroacridine (DMAC), (d) 5,10-dihydrophenazine (DHPZ), and (e) triphenylamine (TPA). The contributions of the HOMO $\rightarrow$ LUMO transition to the S_1 excitation %HL obtained with DLPNO-STEOM-CCSD, are also indicated.

stronger CT character with %HL above 60%, TDDFT excitation energies calculated with the CAM-B3LYP, IP-LC-BLYP, and IP-ωB97X functionals further decrease, to the extent that TDDFT@IP-LC-BLYP excitation energies are underestimated. The decrease of the S_1 excitation energies obtained with the CAM-B3LYP, IP-LC-BLYP, and IP-ωB97X functionals with increasing CT character in Fig. 7(a) stems from the underestimation of CT excitation energies. The more CT-like the excited state is, the more the excitation energy is underestimated relatively to DLPNO-STEOM-CCSD. Because the errors are strongly system dependent and not systematic, the CAM-B3LYP, IP-LC-BLYP, and IP-ωB97X functionals may fail to provide a reliable comparison between the excitation energies of different TADF chromophores. Although the LC-BLYP, ωB97X, ωB2PLYP, and ωB2GP-PLYP functionals significantly overestimate the excitation energies by more than 0.50 eV, the overestimation stays roughly constant and is independent of the degree of CT charac-

ter. Because the errors of these functionals are systematic, they can provide a reliable comparison between different chromophores. This is consistent with yielding the correct excitation energy change as a function of molecular conformation for CzCB, thanks to a balanced description of the relative energies of valence and CT excitations.

Next, we assess the performance of exchange-correlation functionals with respect to the spectral composition of the S_1 excitation. Figure 7(c) shows the difference in the contribution of the HOMO $\rightarrow$ LUMO transition to the S_1 excitation obtained with TDDFT versus the DLPNO-STEOM-CCSD reference Δ%HL. Similarly to the case of CzCB, TDDFT with the CAM-B3LYP, IP-LC-BLYP, and IP-ωB97X functionals underestimates the CT excitation energies and thus overestimates %HL for the benchmark set. %HL is overestimated by 5% to 20% for most molecules owing to the inclusion of only 65% Fock exchange in the long-range in CAM-B3LYP and a range separation parameter ω smaller
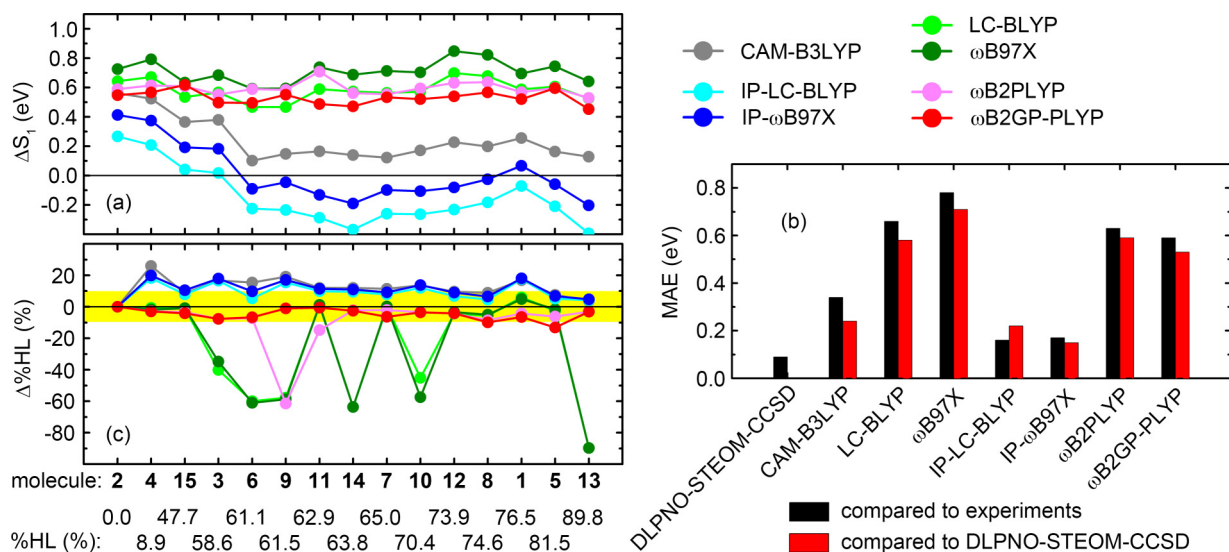
FIG. 7. (a) Difference between the S_1 energies calculated with TDDFT and the DLPNO-STEOM-CCSD reference values; (b) MAEs of S_1 energy referenced to experiments (black) and DLPNO-STEOM-CCSD (red); and (c) difference between %HL obtained with TDDFT and DLPNO-STEOM-CCSD. Molecules are arranged on the x axis in order of increasing %HL, obtained with DLPNO-STEOM-CCSD. Tabulated excitation energies and %HL are provided in the Supplemental Material [135]. The region of $\Delta\%HL$ from -10% to 10% is highlighted in yellow.

than 0.30 bohr^{-1} in IP-LC-BLYP and IP-ωB97X. Tabulated range separation parameters of the IP-LC-BLYP and IP-ωB97X functionals are provided in the Supplemental Material [135]. Considering that with DLPNO-STEOM-CCSD the %HL is generally up to 60% to 80%, an overestimation of 5% to 20% with the CAM-B3LYP, IP-LC-BLYP, and IP-ωB97X functionals corresponds to a strong CT character. For example, for molecule **1** the %HL of 76.5%, obtained with DLPNO-STEOM-CCSD is overestimated by about 18.0%, approaching 95.0%.

With the LC-BLYP, ωB97X, ωB2PLYP, and ωB2GP-PLYP functionals, TDDFT correctly describes the nature of the S_1 excitation of CzCB and its behavior as a function of molecular conformation. The balanced description of CT versus valence transitions, which leads to a correct spectral composition, is also reflected in the TADF benchmark set. However, for some molecules, the LC-BLYP and ωB97X LC hybrid functionals fail in qualitatively predicting the energy ordering between different excited states. As shown in Fig. 7(c), with the LC-BLYP and ωB97X functionals, the %HL of S_1 is severely underestimated for some molecules. For molecule **9**, the %HL of S_1 is also severely underestimated by ωB2PLYP. This is because the excitation energies of CT excited states dominated by the HOMO → LUMO transition are overestimated relative to other valence states, such that the valence states become the lowest excited states. A representative example of molecule **9** is shown in Fig. 8. The excitation energies of the three lowest singlet excited states calculated with DLPNO-STEOM-CCSD are shown on the left side of Fig. 8(a). The CT excited state dominated by the HOMO → LUMO transition is about 0.20 eV lower in energy than the two valence excited states located on either the donor or the acceptor moiety. TDDFT with the LC-BLYP and ωB97X functionals reproduces the spectral composition of these states, similarly to the case of

CzCB. However, the CT state is erroneously predicted to be higher in energy than the two valence states. As shown in Fig. 7(c), a significant fraction of the chromophores studied here suffer from the same issue of incorrect energy ordering of CT versus valence excited states when using the LC-BLYP and ωB97X functionals. Incorrect energy ordering of excited states with TDDFT based on LC-hybrid GGA functionals compared to experiments and DLPNO-STEOM-CCSD, has also been reported for other TADF materials, such as azine derivatives [156]. This problem may be solved by the inclusion of PT2 correlation in range-separated double hybrid functionals. With the ωB2PLYP and ωB2GP-PLYP functionals, most of the chromophores studied here are concentrated within -10% to 10% of the %HL obtained with DLPNO-STEOM-CCSD, in the yellow region of Fig. 7(c). Of the 15 TADF chromophores benchmarked here, an incorrect S_1 state is observed only in molecule **9** with ωB2PLYP. As shown in Fig. 8, the CT excited state of molecule **9** obtained with TDDFT@ωB2PLYP is correctly predicted to be lower in energy than the valence excited state localized on the donor moiety, but still higher than the valence excited state localized on the acceptor moiety. TDDFT@ωB2GP-PLYP yields an accurate spectral composition and the same lowest singlet excited state as DLPNO-STEOM-CCSD for the whole benchmark set. Range-separated double hybrid functionals may thus be used to reliably predict the properties of prospective TADF chromophores. We note, however, that although the energy ordering of the three lowest singlet excited states of molecule **9** obtained with TDDFT@ωB2GP-PLYP reproduces that obtained with DLPNO-STEOM-CCSD, the energy spacing between the three states is different. This calls for further development of more advanced functionals that can qualitatively and *quantitatively* describe the excited-state properties of donor-acceptor molecules. Considering that
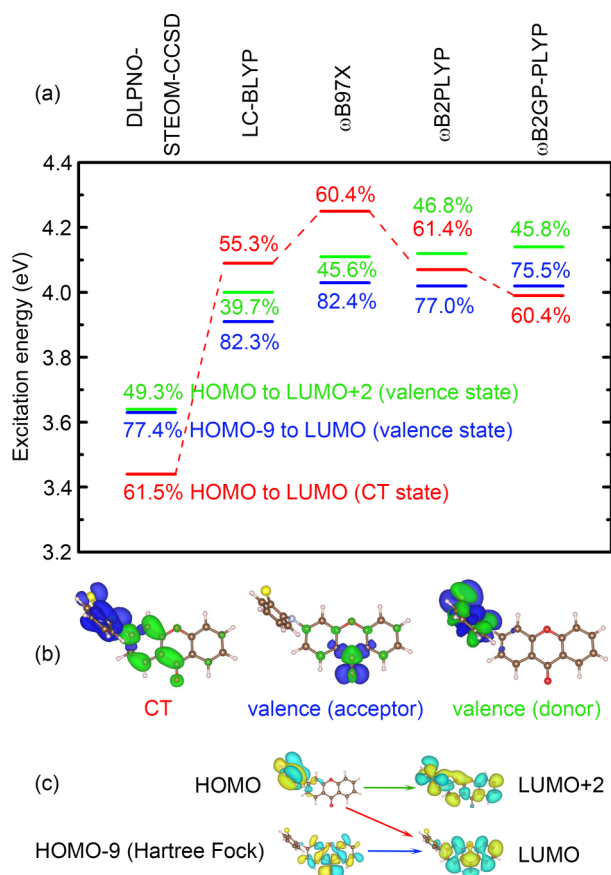
FIG. 8. (a) Energy of the three lowest singlet excited states for molecule **9**, obtained with DLPNO-STEOM-CCSD and TDDFT with the LC-BLYP, ωB97X, ωB2PLYP, and ωB2GP-PLYP functionals. The states dominated by a CT excitation from the PTZ donor to the xanthone (XTN) acceptor, a valence excitation localized on the acceptor, and a valence excitation localized on the donor are indicated by red, blue, and green horizontal lines, respectively. The percentage of contribution of the dominant transitions is also indicated. (b) Electron density differences obtained with TDDFT@ωB2GP-PLYP for the three lowest singlet states with an isosurface value of 0.001 au. The green and blue isosurfaces represent electron gain and electron loss. (c) DFT molecular orbitals corresponding to the dominant transitions contributing to the three lowest singlet states. The HOMO-9 obtained with Hartree Fock corresponds to HOMO-5 with DFT@LC-BLYP, HOMO-6 with DFT@ωB97X, and HOMO-8 with DFT@ωB2PLYP and DFT@ωB2GP-PLYP. The isosurface value is 0.013 au.

the range separation parameters in LC-BLYP, ωB97X, ωB2PLYP, and ωB2GP-PLYP, which correctly predict the spectral composition of excited states, are very close to or equal to each other, this may be achieved by exploring the parameter space of α and β in Eq. (1) and/or introducing range-separated correlation [157].

We note that the CT nature of the singlet excitation and the difference between the first singlet and triplet excitation energies are necessary but not sufficient conditions for efficient TADF. Additional requirements are a long triplet lifetime, a fast RISC rate, and intense fluorescence [5,158,159]. Molecules with very similar ΔE_{ST} may exhibit large vari-

ations in the RISC decay constant [160]. This results from the spin-vibronic coupling, as revealed by quantum dynamics simulations [161] and experimental observations [162]. The spin-vibronic mechanism does not lessen the importance of ΔE_{ST} in TADF. In addition, a small ΔE_{ST} also benefits applications such as TTA upconversion by reducing the energy loss and increasing the anti-Stokes shift [19–21]. The chemical environment may alter the excitation energy and oscillator strength of excited states, affecting TADF efficiency [162–164]. In polar solvents, the RISC decay constant may be significantly enhanced due to stabilized CT states and a smaller ΔE_{ST} [162,164]. Recently, rather than the conventional design of twisted donor-acceptor chromophores, new classes of TADF chromophores have been proposed to meet different requirements. For example, in some molecules that display specific intramolecular noncovalent interactions, a fast RISC from T_1 to S_1 and a fast radiative decay from S_1 to S_0 are simultaneously achieved, facilitating TADF [80]. A design strategy of a rigid polycyclic aromatic framework based on the multiple resonance effect minimizes ΔE_{ST} without broadening of the fluorescence peaks, which improves the color purity of TADF and the external quantum efficiency of OLEDs [30,37,70].

IV. CONCLUSIONS

In summary, TDDFT based on 13 exchange-correlation functionals of different classes was benchmarked for the first singlet excited states of TADF chromophores. The performance of TDDFT was assessed in comparison to experiments and high-level DLPNO-STEOM-CCSD reference data. This enabled us to evaluate not only the accuracy of the excitation energies but also of the spectral composition of the TDDFT excited states. A representative donor-acceptor molecule with a valence S_1 excitation, CzCB, was used as a detailed case study to evaluate whether TDDFT with different functionals erroneously predicts a CT-like excitation. The dihedral angle between the donor and acceptor of CzCB was rotated to vary the degree of spatial separation between the HOMO and LUMO. A set of 15 additional TADF chromophore, whose S_1 excitations have a varying degree of CT character, was further employed to provide statistical data on the performance of TDDFT with range separated hybrid and double hybrid functionals.

Based on the case study of CzCB, we find that TDDFT, using functionals with a globally fixed fraction of Fock exchange, including global hybrid GGA functionals, global hybrid meta-GGA functionals, and double hybrid functionals, underestimates CT excitation energies and may overestimate the CT character of the lowest excited state. This may lead to incorrect predictions of chromophores being potentially promising for TADF. Therefore, these functionals are not considered further. Range separated hybrid and double hybrid functionals with 100% Fock exchange in the long range and a range separation parameter of about 0.30 bohr^{-1}, including LC-BLYP, ωB97X, ωB2PLYP, and ωB2GP-PLYP, are found to provide a balanced description of the valence versus CT nature of the S_1 excited state of CzCB. Range-separated hybrid functionals with different parameters, including CAM-B3LYP with 65% Fock exchange in the long range

and optimally tuned LC hybrid functionals with smaller range separation parameters, may fail owing to an insufficient fraction of Fock exchange.

Based on the benchmark set of 15 TADF chromophores, we find that TDDFT using the LC-BLYP, ωB97X, ωB2PLYP, and ωB2GP-PLYP functionals systematically significantly overestimates the S_1 excitation energies. In contrast, with the CAM-B3LYP, IP-LC-BLYP, and IP-ωB97X functionals the errors are not systematic, but rather a function of the degree of CT character of the S_1 excitation. With CAM-B3LYP the overestimation of the S_1 excitation energies decreases with increasing CT character, whereas with IP-LC-BLYP, and IP-ωB97X the errors in the S_1 excitation energies change from overestimation for a low CT character to underestimation for a high CT character. This means that the CAM-B3LYP, IP-LC-BLYP, and IP-ωB97X functionals cannot be used to reliably compare between different prospective TADF chromophores. TDDFT@LC-BLYP and TDDFT@ωB97X produce an incorrect energy ordering of different CT and valence excited states for some molecules. This problem is rectified by the inclusion of PT2 correlation in range-separated double hybrid functionals, which yield an accurate spectral compositions of excited states and correct energy ordering of CT and valence excited states, compared to DLPNO-STEOM-CCSD.

In conclusion, TDDFT is appealing for excited-state simulations of molecules thanks to its efficiency, compared to computationally expensive high-level quantum chemistry methods, which enables screening a large number of candidates. However, the reliability of TDDFT strongly depends on the choice of the exchange-correlation functional. Based on the findings reported here, we recommend range-separated double hybrid functionals, in particular the ωB2GP-PLYP functional, for TDDFT calculations of potential TADF chromophores. Although range-separated double hybrid functionals are demonstrated here to provide qualitatively accurate results, the excitation energies and energy spacings between different excited states need to be further *quantitatively* improved. This may be achieved by exploring the parameter space of Fock exchange and PT2 correlation fractions and/or introducing range-separated correlation. These findings are important for our ability to reliably predict the properties of donor-acceptor molecules to advance the development of highly efficient OLEDs with TADF. In addition, they would benefit computational materials discovery efforts for other applications involving intramolecular CT states.

[1] O. Ostroverkhova, Organic optoelectronic materials: Mechanisms and applications, Chem. Rev. **116**, 13279 (2016).

[2] Y.-W. Su, S.-C. Lan, and K.-H. Wei, Organic photovoltaics, Mater. Today **15**, 554 (2012).

[3] S.-J. Zou, Y. Shen, F.-M. Xie, J.-D. Chen, Y.-Q. Li, and J.-X. Tang, Recent advances in organic light-emitting diodes: Toward smart lighting and displays, Mater. Chem. Front. **4**, 788 (2020).

[4] S. Reineke, M. Thomschke, B. Lüssem, and K. Leo, White organic light-emitting diodes: Status and perspective, Rev. Mod. Phys. **85**, 1245 (2013).

[5] Z. Yang, Z. Mao, Z. Xie, Y. Zhang, S. Liu, J. Zhao, J. Xu, Z. Chi, and M. P. Aldred, Recent advances in organic thermally activated delayed fluorescence materials, Chem. Soc. Rev. **46**, 915 (2017).

[6] B. Wex and B. R. Kaafarani, Perspective on carbazole-based organic compounds as emitters and hosts in TADF applications, J. Mater. Chem. C **5**, 8622 (2017).

[7] M. Y. Wong and E. Zysman-Colman, Purely organic thermally activated delayed fluorescence materials for organic light-emitting diodes, Adv. Mater. **29**, 1605444 (2017).

[8] Y. Liu, C. Li, Z. Ren, S. Yan, and M. R. Bryce, All-organic thermally activated delayed fluorescence materials for organic light-emitting diodes, Nat. Rev. Mater. **3**, 18020 (2018).

[9] T. Huang, W. Jiang, and L. Duan, Recent progress in solution processable TADF materials for organic light-emitting diodes, J. Mater. Chem. C **6**, 5577 (2018).

[10] X. Cai and S.-J. Su, Marching toward highly efficient, pure-blue, and stable thermally activated delayed fluorescent organic light-emitting diodes, Adv. Funct. Mater. **28**, 1802558 (2018).

[11] C. A. Parker and C. G. Hatchard, Triplet-singlet emission in fluid solutions. Phosphorescence of eosin, Trans. Faraday Soc. **57**, 1894 (1961).

[12] A. Endo, K. Sato, K. Yoshimura, T. Kai, A. Kawada, H. Miyazaki, and C. Adachi, Efficient up-conversion of triplet excitons into a singlet state and its application for organic light emitting diodes, Appl. Phys. Lett. **98**, 083302 (2011).

[13] R. Pollice, P. Friederich, C. Lavigne, G. dos Passos Gomes, and A. Aspuru-Guzik, Organic molecules with inverted gaps between first excited singlet and triplet states and appreciable fluorescence rates, Matter **4**, 1654 (2021).

[14] J.-M. Teng, Y.-F. Wang, and C.-F. Chen, Recent progress of narrowband TADF emitters and their applications in OLEDs, J. Mater. Chem. C **8**, 11340 (2020).

[15] G. U. Mahoro, J. Fernandez-Cestau, J.-L. Renaud, P. B. Coto, R. D. Costa, and S. Gaillard, Recent advances in solid-state lighting devices using transition metal complexes exhibiting

thermally activated delayed fluorescent emission mechanism, Adv. Opt. Mater. **8**, 2000260 (2020).

[16] A. Endo, M. Ogasawara, A. Takahashi, D. Yokoyama, Y. Kato, and C. Adachi, Thermally activated delayed fluorescence from Sn4+-porphyrin complexes and their application to organic light emitting diodes—A novel mechanism for electroluminescence, Adv. Mater. **21**, 4802 (2009).

[17] J. C. Deaton, S. C. Switalski, D. Y. Kondakov, R. H. Young, T. D. Pawlik, D. J. Giesen, S. B. Harkins, A. J. M. Miller, S. F. Mickenberg, and J. C. Peters, E-type delayed fluorescence of a phosphine-supported $Cu_2(mu-NAr_2)_2$ diamond core: Harvesting singlet and triplet excitons in OLEDs, J. Am. Chem. Soc. **132**, 9499 (2010).

[18] Y. Zhu, Y. Zhang, B. Yao, Y. Wang, Z. Zhang, H. Zhan, B. Zhang, Z. Xie, Y. Wang, and Y. Cheng, Synthesis and electroluminescence of a conjugated polymer with thermally activated delayed fluorescence, Macromolecules **49**, 4373 (2016).

[19] X. Wang, R. Tom, X. Liu, D. N. Congreve, and N. Marom, An energetic perspective on why there are so few triplet-triplet annihilation emitters, J. Mater. Chem. C **8**, 10816 (2020).

[20] N. Yanai, M. Kozue, S. Amemori, R. Kabe, C. Adachi, and N. Kimizuka, Increased vis-to-uv upconversion performance by energy level matching between a TADF donor and high triplet energy acceptors, J. Mater. Chem. C **4**, 6447 (2016).

[21] X. Wang and N. Marom, An energetics assessment of benzo[*a*]tetracene and benzo[*a*]pyrene as triplet-triplet annihilation emitters, Mol. Syst. Des. Eng. **7**, 889 (2022).

[22] X.-K. Chen, D. Kim, and J.-L. Brédas, Thermally activated delayed fluorescence (TADF) path toward efficient electroluminescence in purely organic materials: Molecular level insight, Acc. Chem. Res. **51**, 2215 (2018).

[23] S. Hirata, Y. Sakai, K. Masui, H. Tanaka, S. Y. Lee, H. Nomura, N. Nakamura, M. Yasumatsu, H. Nakanotani, Q. Zhang *et al.*, Highly efficient blue electroluminescence based on thermally activated delayed fluorescence, Nat. Mater. **14**, 330 (2015).

[24] S. Y. Lee, T. Yasuda, I. S. Park, and C. Adachi, X-shaped benzoylbenzophenone derivatives with crossed donors and acceptors for highly efficient thermally activated delayed fluorescence, Dalton Trans. **44**, 8356 (2015).

[25] K. Kawasumi, T. Wu, T. Zhu, H. S. Chae, T. Van Voorhis, M. A. Baldo, and T. M. Swager, Thermally activated delayed fluorescence materials based on homoconjugation effect of donor-acceptor triptycenes, J. Am. Chem. Soc. **137**, 11908 (2015).

[26] Z. Xie, C. Chen, S. Xu, J. Li, Y. Zhang, S. Liu, J. Xu, and Z. Chi, White-light emission strategy of a single organic compound with aggregation-induced emission and delayed fluorescence properties, Angew. Chem., Int. Ed. **54**, 7181 (2015).

[27] H. Uoyama, K. Goushi, K. Shizu, H. Nomura, and C. Adachi, Highly efficient organic light-emitting diodes from delayed fluorescence, Nature (London) **492**, 234 (2012).

[28] Q. Zhang, B. Li, S. Huang, H. Nomura, H. Tanaka, and C. Adachi, Efficient blue organic light-emitting diodes employing thermally activated delayed fluorescence, Nat. Photonics **8**, 326 (2014).

[29] T. Vikramaditya, M. Saisudhakar, and K. Sumithra, Computational study on thermally activated delayed fluorescence of donor-linker-acceptor network molecules, RSC Adv. **6**, 37203 (2016).

[30] D. Hall, S. M. Suresh, P. L. dos Santos, E. Duda, S. Bagnich, A. Pershin, P. Rajamalli, D. B. Cordes, A. M. Z. Slawin, D. Beljonne *et al.*, Improving processability and efficiency of resonant TADF emitters: A design strategy, Adv. Opt. Mater. **8**, 1901627 (2020).

[31] D. Sun, S. M. Suresh, D. Hall, M. Zhang, C. Si, D. B. Cordes, A. M. Z. Slawin, Y. Olivier, X. Zhang, and E. Zysman-Colman, The design of an extended multiple resonance tadf emitter based on a polycyclic amine/carbonyl system, Mater. Chem. Front. **4**, 2018 (2020).

[32] H. Sun, C. Zhong, and J.-L. Brédas, Reliable prediction with tuned range-separated functionals of the singlet-triplet gap in organic emitters for thermally activated delayed fluorescence, J. Chem. Theory Comput. **11**, 3851 (2015).

[33] Y. Zou, S. Gong, G. Xie, and C. Yang, Design strategy for solution-processable thermally activated delayed fluorescence emitters and their applications in organic light-emitting diodes, Adv. Opt. Mater. **6**, 1800568 (2018).

[34] Y. Tao, K. Yuan, T. Chen, P. Xu, H. Li, R. Chen, C. Zheng, L. Zhang, and W. Huang, Thermally activated delayed fluorescence materials towards the breakthrough of organoelectronics, Adv. Mater. **26**, 7931 (2014).

[35] P. de Silva, C. A. Kim, T. Zhu, and T. Van Voorhis, Extracting design principles for efficient thermally activated delayed fluorescence (TADF) from a simple four-state model, Chem. Mater. **31**, 6995 (2019).

[36] A. Hellweg, S. A. Grun, and C. Hattig, Benchmarking the performance of spin-component scaled CC2 in ground and electronically excited states, Phys. Chem. Chem. Phys. **10**, 4119 (2008).

[37] A. Pershin, A. Pershin, V. Lemaur, J.-C. Sancho-Garcia, L. Muccioli, E. Zysman-Colman, D. Beljonne, and Y. Olivier, Highly emissive excitons with reduced exchange energy in thermally activated delayed fluorescent molecules, Nat. Commun. **10**, 597 (2019).

[38] C. Riplinger and F. Neese, An efficient and near linear scaling pair natural orbital based local coupled cluster method, J. Chem. Phys. **138**, 034106 (2013).

[39] C. Riplinger, B. Sandhoefer, A. Hansen, and F. Neese, Natural triple excitations in local coupled cluster calculations with pair natural orbitals, J. Chem. Phys. **139**, 134101 (2013).

[40] M. Nooijen and R. J. Bartlett, A new method for excited states: Similarity transformed equation-of-motion coupled-cluster theory, J. Chem. Phys. **106**, 6441 (1997).

[41] E. Runge and E. K. U. Gross, Density-Functional Theory for Time-Dependent Systems, Phys. Rev. Lett. **52**, 997 (1984).

[42] W. Liu and Y. Xiao, Relativistic time-dependent density functional theories, Chem. Soc. Rev. **47**, 4481 (2018).

[43] R. Gómez-Bombarelli, J. Aguilera-Iparraguirre, T. D. Hirzel, D. Duvenaud, D. Maclaurin, M. A. Blood-Forsythe, H. S. Chae, M. Einzinger, D.-G. Ha, T. Wu *et al.*, Design of efficient molecular organic light-emitting diodes by a high-throughput virtual screening and experimental approach, Nat. Mater. **15**, 1120 (2016).

[44] S. Kümmel, Charge-transfer excitations: A challenge for time-dependent density functional theory that has been met, Adv. Energy Mater. **7**, 1700440 (2017).

[45] T. Körzdörfer, S. Kümmel, N. Marom, and L. Kronik, When to trust photoelectron spectra from Kohn-Sham eigenvalues: The case of organic semiconductors, Phys. Rev. B **79**, 201205(R) (2009).

[46] Y. Zhang and W. Yang, A challenge for density functionals: Self-interaction error increases for systems with a noninteger number of electrons, J. Chem. Phys. **109**, 2604 (1998).

[47] P. Mori-Sánchez, A. J. Cohen, and W. Yang, Many-electron self-interaction error in approximate density functionals, J. Chem. Phys. **125**, 201102 (2006).

[48] A. Dreuw and M. Head-Gordon, Failure of time-dependent density functional theory for long-range charge-transfer excited states: The zincbacteriochlorin-bacteriochlorin and bacteriochlorophyll-spheroidene complexes, J. Am. Chem. Soc. **126**, 4007 (2004).

[49] O. Gritsenko and E. J. Baerends, Asymptotic correction of the exchange-correlation kernel of time-dependent density functional theory for long-range charge-transfer excitations, J. Chem. Phys. **121**, 655 (2004).

[50] Y. Yamaguchi, Y. Yokomichi, S. Yokoyama, and S. Mashiko, Time-dependent density functional calculations of the Q-like bands of phenylene-linked free-base and zinc porphyrin dimers, Int. J. Quantum Chem. **84**, 338 (2001).

[51] Y. Yamaguchi, S. Yokoyama, and S. Mashiko, Strong coupling of the single excitations in the Q-like bands of phenylene-linked free-base and zinc bacteriochlorin dimers: A time-dependent density functional theory study, J. Chem. Phys. **116**, 6541 (2002).

[52] N. T. Maitra, Charge transfer in time-dependent density functional theory, J. Phys.: Condens. Matter **29**, 423001 (2017).

[53] B. Alam, A. F. Morrison, and J. M. Herbert, Charge separation and charge transfer in the low-lying excited states of pentacene, J. Phys. Chem. C **124**, 24653 (2020).

[54] T. Yanai, D. P. Tew, and N. C. Handy, A new hybrid exchange-correlation functional using the Coulomb-attenuating method (CAM-B3LYP), Chem. Phys. Lett. **393**, 51 (2004).

[55] H. Iikura, T. Tsuneda, T. Yanai, and K. Hirao, A long-range correction scheme for generalized-gradient-approximation exchange functionals, J. Chem. Phys. **115**, 3540 (2001).

[56] J.-D. Chai and M. Head-Gordon, Systematic optimization of long-range corrected hybrid density functionals, J. Chem. Phys. **128**, 084106 (2008).

[57] S. Kanchanakungwankul and D. G. Truhlar, Examination of how well long-range-corrected density functionals satisfy the ionization energy theorem, J. Chem. Theory Comput. **17**, 4823 (2021).

[58] G. Santra, M. Cho, and J. M. L. Martin, Exploring avenues beyond revised dsd functionals: I. Range separation, with xDSD as a special case, J. Phys. Chem. A **125**, 4614 (2021).

[59] O. A. Vydrov and G. E. Scuseria, Assessment of a long-range corrected hybrid functional, J. Chem. Phys. **125**, 234109 (2006).

[60] M. A. Rohrdanz, K. M. Martins, and J. M. Herbert, A long-range-corrected density functional that performs well for both ground-state properties and time-dependent density functional theory excitation energies, including charge-transfer excited states, J. Chem. Phys. **130**, 054112 (2009).

[61] T. Le Bahers, C. Adamo, and I. Ciofini, A qualitative index of spatial extent in charge-transfer excitations, J. Chem. Theory Comput. **7**, 2498 (2011).

[62] S. Zheng, E. Geva, and B. D. Dunietz, Solvated charge transfer states of functionalized anthracene and tetracyanoethylene dimers: A computational study based on a range separated hybrid functional and charge constrained self-consistent field with switching gaussian polarized continuum models, J. Chem. Theory Comput. **9**, 1125 (2013).

[63] T. Stein, L. Kronik, and R. Baer, Reliable prediction of charge transfer excitations in molecular complexes using time-dependent density functional theory, J. Am. Chem. Soc. **131**, 2818 (2009).

[64] T. Körzdörfer and J.-L. Brédas, Organic electronic materials: Recent advances in the dft description of the ground and excited states using tuned range-separated hybrid functionals, Acc. Chem. Res. **47**, 3284 (2014).

[65] W. J. Park, Y. Lee, J. Y. Kim, D. W. Yoon, J. Kim, S. H. Chae, H. Kim, G. Lee, S. Shim, J. H. Yang, and S. J. Lee, Effective thermally activated delayed fluorescence emitter and its performance in OLED device, Synth. Met. **209**, 99 (2015).

[66] P. J. Stephens, F. J. Devlin, C. F. Chabalowski, and M. J. Frisch, *Ab initio* calculation of vibrational absorption and circular dichroism spectra using density functional force fields, J. Phys. Chem. **98**, 11623 (1994).

[67] C. Adamo and V. Barone, Toward reliable density functional methods without adjustable parameters: The PBE0 model, J. Chem. Phys. **110**, 6158 (1999).

[68] J. Li, T. Nakagawa, J. MacDonald, Q. Zhang, H. Nomura, H. Miyazaki, and C. Adachi, Highly efficient organic light-emitting diode based on a hidden thermally activated delayed fluorescence channel in a heptazine derivative, Adv. Mater. **25**, 3319 (2013).

[69] S. Y. Lee, T. Yasuda, Y. S. Yang, Q. Zhang, and C. Adachi, Luminous butterflies: Efficient exciton harvesting by benzophenone derivatives for full-color delayed fluorescence OLEDs, Angew. Chem., Int. Ed. **126**, 6520 (2014).

[70] T. Hatakeyama, K. Shiren, K. Nakajima, S. Nomura, S. Nakatsuka, K. Kinoshita, J. Ni, Y. Ono, and T. Ikuta, Ultra-pure blue thermally activated delayed fluorescence molecules: Efficient HOMO-LUMO separation by the multiple resonance effect, Adv. Mater. **28**, 2777 (2016).

[71] H. Tanaka, K. Shizu, H. Miyazaki, and C. Adachi, Efficient green thermally activated delayed fluorescence (TADF) from a phenoxazine-triphenyltriazine (PXZ-TRZ) derivative, Chem. Commun. **48**, 11392 (2012).

[72] K. Sato, K. Shizu, K. Yoshimura, A. Kawada, H. Miyazaki, and C. Adachi, Organic Luminescent Molecule with Energetically Equivalent Singlet and Triplet Excited States for Organic Light-Emitting Diodes, Phys. Rev. Lett. **110**, 247401 (2013).

[73] D. Zhang, M. Cai, Y. Zhang, D. Zhang, and L. Duan, Sterically shielded blue thermally activated delayed fluorescence emitters with improved efficiency and stability, Mater. Horiz. **3**, 145 (2016).

[74] X. Wang, Y. Sun, G. Wang, J. Li, X. Li, and K. Zhang, TADF-type organic afterglow, Angew. Chem. Int. Ed. **60**, 17138 (2021).

[75] M. Li, Y.-F. Wang, D. Zhang, L. Duan, and C.-F. Chen, Axially chiral TADF-active enantiomers designed for efficient blue

circularly polarized electroluminescence, Angew. Chem. Int. Ed. **59**, 3500 (2020).

[76] L. Yu, Z. Wu, G. Xie, W. Zeng, D. Ma, and C. Yang, Molecular design to regulate the photophysical properties of multifunctional TADF emitters towards high-performance TADF-based OLEDs with EQEs up to 22.4 small efficiency roll-offs, Chem. Sci. **9**, 1385 (2018).

[77] K. Zheng, F. Ni, Z. Chen, C. Zhong, and C. Yang, Polymorph-dependent thermally activated delayed fluorescence emitters: Understanding TADF from a perspective of aggregation state, Angew. Chem. Int. Ed. **59**, 9972 (2020).

[78] E. Spuling, N. Sharma, I. D. W. Samuel, E. Zysman-Colman, and S. Bräse, (Deep) blue through-space conjugated TADF emitters based on [2.2]paracyclophanes, Chem. Commun. **54**, 9278 (2018).

[79] L. Zhan, Z. Chen, S. Gong, Y. Xiang, F. Ni, X. Zeng, G. Xie, and C. Yang, A simple organic molecule realizing simultaneous TADF, RTP, AIE, and mechanoluminescence: Understanding the mechanism behind the multifunctional emitter, Angew. Chem. Int. Ed. **58**, 17651 (2019).

[80] X.-K. Chen, B. W. Bakr, M. Auffray, Y. Tsuchiya, C. D. Sherrill, C. Adachi, and J.-L. Bredas, Intramolecular noncovalent interactions facilitate thermally activated delayed fluorescence (TADF), J. Phys. Chem. Lett. **10**, 3260 (2019).

[81] K. Shizu, H. Noda, H. Tanaka, M. Taneda, M. Uejima, T. Sato, K. Tanaka, H. Kaji, and C. Adachi, Highly efficient blue electroluminescence using delayed-fluorescence emitters with large overlap density between luminescent and ground states, J. Phys. Chem. C **119**, 26283 (2015).

[82] W. Li, Y. Pan, R. Xiao, Q. Peng, S. Zhang, D. Ma, F. Li, F. Shen, Y. Wang, B. Yang, and Y. Ma, Employing 100% excitons in OLEDs by utilizing a fluorescent molecule with hybridized local and charge-transfer excited state, Adv. Funct. Mater. **24**, 1609 (2014).

[83] Y. Zhao and D. G. Truhlar, The M06 suite of density functionals for main group thermochemistry, thermochemical kinetics, noncovalent interactions, excited states, and transition elements: Two new functionals and systematic testing of four M06-class functionals and 12 other functionals, Theor. Chem. Acc. **120**, 215 (2008).

[84] J.-D. Chai and M. Head-Gordon, Long-range corrected hybrid density functionals with damped atom-atom dispersion corrections, Phys. Chem. Chem. Phys. **10**, 6615 (2008).

[85] M. Casanova-Páez and L. Goerigk, Global double hybrids do not work for charge transfer: A comment on double hybrids and time-dependent density functional theory: An implementation and benchmark on charge transfer excited states, J. Comput. Chem. **42**, 528 (2021).

[86] D. Jacquemin, V. Wathelet, E. A. Perpète, and C. Adamo, Extensive TD-DFT benchmark: Singlet-excited states of organic molecules, J. Chem. Theory Comput. **5**, 2420 (2009).

[87] A. D. Laurent and D. Jacquemin, TD-DFT benchmarks: A review, Int. J. Quantum Chem. **113**, 2019 (2013).

[88] S. S. Leang, F. Zahariev, and M. S. Gordon, Benchmarking the performance of time-dependent density functional methods, J. Chem. Phys. **136**, 104101 (2012).

[89] M. Pastore, E. Mosconi, F. De Angelis, and M. Grätzel, A computational investigation of organic dyes for dye-sensitized solar cells: Benchmark, strategies, and open issues, J. Phys. Chem. C **114**, 7205 (2010).

[90] L. Goerigk, J. Moellmann, and S. Grimme, Computation of accurate excitation energies for large organic molecules with double-hybrid density functionals, Phys. Chem. Chem. Phys. **11**, 4611 (2009).

[91] B. Suo, K. Shen, Z. Li, and W. Liu, Performance of TD-DFT for excited states of open-shell transition metal compounds, J. Phys. Chem. A **121**, 3929 (2017).

[92] R. J. Magyar and S. Tretiak, Dependence of spurious charge-transfer excited states on orbital exchange in TDDFT: Large molecules and clusters, J. Chem. Theory Comput. **3**, 976 (2007).

[93] J. Plötner, D. J. Tozer, and A. Dreuw, Dependence of excited state potential energy surfaces on the spatial overlap of the Kohn-Sham orbitals and the amount of nonlocal Hartree-Fock exchange in time-dependent density functional theory, J. Chem. Theory Comput. **6**, 2315 (2010).

[94] B. Moore, H. Sun, N. Govind, K. Kowalski, and J. Autschbach, Charge-transfer versus charge-transfer-like excitations revisited, J. Chem. Theory Comput. **11**, 3305 (2015).

[95] D. Mester and M. Kállay, Charge-transfer excitations within density functional theory: How accurate are the most recommended approaches? J. Chem. Theory Comput. **18**, 1646 (2022).

[96] M. Casanova-Páez and L. Goerigk, Time-dependent long-range-corrected double-hybrid density functionals with spin-component and spin-opposite scaling: A comprehensive analysis of singlet-singlet and singlet-triplet excitation energies, J. Chem. Theory Comput. **17**, 5165 (2021).

[97] E. Bremond, A. Ottochian, A. J. Perez-Jimenez, I. Ciofini, G. Scalmani, M. J. Frisch, J. C. Sancho-Garcia, and C. Adamo, Assessing challenging intra- and inter-molecular charge-transfer excitations energies with double-hybrid density functionals, J. Comput. Chem. **42**, 970 (2021).

[98] P.-F. Loos, M. Comin, X. Blase, and D. Jacquemin, Reference energies for intramolecular charge-transfer excitations, J. Chem. Theory Comput. **17**, 3666 (2021).

[99] M. Moral, L. Muccioli, W.-J. Son, Y. Olivier, and J. C. Sancho-García, Theoretical rationalization of the singlet-triplet gap in OLEDs materials: Impact of charge-transfer character, J. Chem. Theory Comput. **11**, 168 (2015).

[100] T. J. Penfold, On predicting the excited-state properties of thermally activated delayed fluorescence emitters, J. Phys. Chem. C **119**, 13535 (2015).

[101] K. Liang, C. Zheng, K. Wang, W. Liu, Z. Guo, Y. Li, and X. Zhang, Theoretical investigation of the singlet-triplet splittings for carbazole-based thermally activated delayed fluorescence emitters, Phys. Chem. Chem. Phys. **18**, 26623 (2016).

[102] S. Huang, Q. Zhang, Y. Shiota, T. Nakagawa, K. Kuwabara, K. Yoshizawa, and C. Adachi, Computational prediction for singlet- and triplet-transition energies of charge-transfer compounds, J. Chem. Theory Comput. **9**, 3872 (2013).

[103] M. J. G. Peach, M. J. Williamson, and D. J. Tozer, Influence of triplet instabilities in TDDFT, J. Chem. Theory Comput. **7**, 3578 (2011).

[104] M. J. G. Peach and D. J. Tozer, Overcoming low orbital overlap and triplet instability problems in TDDFT, J. Phys. Chem. A **116**, 9783 (2012).

[105] J. S. Sears, T. Koerzdoerfer, C.-R. Zhang, and J.-L. Brédas, Communication: Orbital instabilities and triplet states from

time-dependent density functional theory and long-range corrected functionals, J. Chem. Phys. **135**, 151103 (2011).

[106] R. Berraud-Pache, F. Neese, G. Bistoni, and R. Izsák, Unveiling the photophysical properties of boron-dipyrromethene dyes using a new accurate excited state coupled cluster method, J. Chem. Theory Comput. **16**, 564 (2020).

[107] A. K. Dutta, M. Saitow, C. Riplinger, F. Neese, and R. Izsak, A near-linear scaling equation of motion coupled cluster method for ionized states, J. Chem. Phys. **148**, 244101 (2018).

[108] A. K. Dutta, M. Saitow, B. Demoulin, F. Neese, and R. Izsák, A domain-based local pair natural orbital implementation of the equation of motion coupled cluster method for electron attached states, J. Chem. Phys. **150**, 164123 (2019).

[109] A. K. Dutta, F. Neese, and R. Izsak, Towards a pair natural orbital coupled cluster method for excited states, J. Chem. Phys. **145**, 034102 (2016).

[110] A. K. Dutta, M. Nooijen, F. Neese, and R. Izsak, Exploring the accuracy of a low scaling similarity transformed equation of motion method for vertical excitation energies, J. Chem. Theory Comput. **14**, 72 (2018).

[111] M. Schreiber, M. R. Silva-Junior, S. P. A. Sauer, and W. Thiel, Benchmarks for electronically excited states: CASPT2, CC2, CCSD, and CC3, J. Chem. Phys. **128**, 134110 (2008).

[112] J. P. Perdew and K. Schmidt, Jacob's ladder of density functional approximations for the exchange-correlation energy, AIP Conf. Proc. **577**, 1 (2001).

[113] V. N. Staroverov, G. E. Scuseria, J. Tao, and J. P. Perdew, Comparative assessment of a new nonempirical density functional: Molecules and hydrogen-bonded complexes, J. Chem. Phys. **119**, 12129 (2003).

[114] S. Grimme, Semiempirical hybrid density functional with perturbative second-order correlation, J. Chem. Phys. **124**, 034108 (2006).

[115] A. Karton, A. Tarnopolsky, J.-F. Lamère, G. C. Schatz, and J. M. L. Martin, Highly accurate first-principles benchmark data sets for the parametrization and validation of density functional and other approximate methods. derivation of a robust, generally applicable, double-hybrid functional for thermochemistry and thermochemical kinetics, J. Phys. Chem. A **112**, 12868 (2008).

[116] M. Casanova-Páez, M. B. Dardis, and L. Goerigk, wB2PLYP and wB2GPPLYP: The first two double-hybrid density functionals with long-range correction optimized for excitation energies, J. Chem. Theory Comput. **15**, 4735 (2019).

[117] A. Görling and M. Levy, Correlation-energy functional and its high-density limit obtained from a coupling-constant perturbation expansion, Phys. Rev. B **47**, 13105 (1993).

[118] A. Görling and M. Levy, Exact Kohn-Sham scheme based on perturbation theory, Phys. Rev. A **50**, 196 (1994).

[119] P. Mori-Sanchez, Q. Wu, and W. Yang, Orbital-dependent correlation energy in density-functional theory based on a second-order perturbation approach: Success and failure, J. Chem. Phys. **123**, 062204 (2005).

[120] Y. Wang, Y. Li, J. Chen, I. Y. Zhang, and X. Xu, Doubly hybrid functionals close to chemical accuracy for both finite and extended systems: Implementation and test of XYG3 and XYGJ-OS, JACS Au **1**, 543 (2021).

[121] D. Jayatilaka and A. Karton, The *duhka* of DFT: A noble path to better functionals via a point electron approximation for the exchange-correlation hole, Aust. J. Chem. (2022), doi: 10.1071/CH21332.

[122] B. Miehlich, A. Savin, H. Stoll, and H. Preuss, Results obtained with the correlation energy density functionals of Becke and Lee, Yang and Parr, Chem. Phys. Lett. **157**, 200 (1989).

[123] A. D. Becke, Density-functional thermochemistry. V. Systematic optimization of exchange-correlation functionals, J. Chem. Phys. **107**, 8554 (1997).

[124] T. Koopmans, Über die zuordnung von wellenfunktionen und eigenwerten zu den einzelnen elektronen eines atoms, Physica **1**, 104 (1934).

[125] F. Neese, The ORCA program system, WIREs Comput. Mol. Sci. **2**, 73 (2012).

[126] S. Grimme, S. Ehrlich, and L. Goerigk, Effect of the damping function in dispersion corrected density functional theory, J. Comput. Chem. **32**, 1456 (2011).

[127] F. Weigend and R. Ahlrichs, Balanced basis sets of split valence, triple zeta valence and quadruple zeta valence quality for H to Rn: Design and assessment of accuracy, Phys. Chem. Chem. Phys. **7**, 3297 (2005).

[128] M. H. Lechner, F. Neese, and R. Izsak, An excited state coupled-cluster study on indigo dyes, Mol. Phys. **119**, e1965235 (2021).

[129] A. Hellweg, C. Hättig, S. Höfener, and W. Klopper, Optimized accurate auxiliary basis sets for RI-MP2 and RI-CC2 calculations for the atoms Rb to Rn, Theor. Chem. Acc. **117**, 587 (2007).

[130] W. Tang, E. Sanville, and G. Henkelman, A grid-based Bader analysis algorithm without lattice bias, J. Phys.: Condens. Matter **21**, 084204 (2009).

[131] M. Yu and D. R. Trinkle, Accurate and efficient algorithm for Bader charge integration, J. Chem. Phys. **134**, 064111 (2011).

[132] V. Blum, R. Gehrke, F. Hanke, P. Havu, V. Havu, X. Ren, K. Reuter, and M. Scheffler, *Ab initio* molecular simulations with numeric atom-centered orbitals, Comput. Phys. Commun. **180**, 2175 (2009).

[133] V. Havu, V. Blum, P. Havu, and M. Scheffler, Efficient o(n) integration for all-electron electronic structure calculation using numeric basis functions, J. Comput. Phys. **228**, 8367 (2009).

[134] X. Ren, P. Rinke, V. Blum, J. Wieferink, A. Tkatchenko, A. Sanfilippo, K. Reuter, and M. Scheffler, Resolution-of-identity approach to Hartree-Fock, hybrid density functionals, RPA, MP2 and *GW* with numeric atom-centered orbital basis functions, New J. Phys. **14**, 053020 (2012).

[135] See Supplemental Material at http://link.aps.org/supplemental/10.1103/PhysRevResearch.4.033147 for the "Jacob's ladder" of density functional approximations, the basis sets convergence test for CzCB, orbitals of CzCB, the spectral composition of the lowest singlet excited state for CzCB, chemical names and frontier orbitals of the benchmark set, and excitation energies of the benchmark set.

[136] B. M. Wong and T. H. Hsieh, Optoelectronic and excitonic properties of oligoacenes: Substantial improvements from range-separated time-dependent density functional theory, J. Chem. Theory Comput. **6**, 3704 (2010).

[137] A. E. Raeber and B. M. Wong, The importance of short- and long-range exchange on various excited state properties of DNA monomers, stacked complexes, and Watson-Crick pairs, J. Chem. Theory Comput. **11**, 2199 (2015).

[138] J.-W. Song and K. Hirao, What makes differences between intra- and inter-molecular charge transfer excitations in conjugated long-chained polyene? EOM-CCSD and LC-BOP study, Theor. Chem. Acc. **133**, 1438 (2014).

[139] L. Goerigk and S. Grimme, Assessment of TD-DFT methods and of various spin scaled CIS(D) and CC2 versions for the treatment of low-lying valence excitations of large organic dyes, J. Chem. Phys. **132**, 184103 (2010).

[140] D. Jacquemin, B. Moore, A. Planchat, C. Adamo, and J. Autschbach, Performance of an optimally tuned range-separated hybrid functional for 0-0 electronic excitation energies, J. Chem. Theory Comput. **10**, 1677 (2014).

[141] S. Refaely-Abramson, R. Baer, and L. Kronik, Fundamental and excitation gaps in molecules of relevance for organic photovoltaics from an optimally tuned range-separated hybrid functional, Phys. Rev. B **84**, 075144 (2011).

[142] L. Kronik, T. Stein, S. Refaely-Abramson, and R. Baer, Excitation gaps of finite-sized systems from optimally tuned range-separated hybrid functionals, J. Chem. Theory Comput. **8**, 1515 (2012).

[143] A. Karolewski, L. Kronik, and S. Kümmel, Using optimally tuned range separated hybrid functionals in ground-state calculations: Consequences and caveats, J. Chem. Phys. **138**, 204115 (2013).

[144] D. Y. Kwon, G. H. Lee, and Y. S. Kim, Theoretical study of xanthenone and phenothiazine derivatives for blue TADF emitter, Mol. Cryst. Liq. Cryst. **620**, 166 (2015).

[145] D. Y. Kwon, G. H. Lee, and Y. S. Kim, Study of an oxadiazole derivative for a blue thermally activated delayed fluorescence emitter, J. Nanosci. Nanotechnol. **15**, 7828 (2015).

[146] B. Huang, Z. Yin, X. Ban, W. Jiang, Y. Dai, J. Zhang, Y. Liu, Y. Yang, and Y. Sun, Thermally activated delayed fluorescence of n-phenylcarbazole and triphenylamine functionalised tris(aryl)triazines, Dyes and Pigments **117**, 141 (2015).

[147] Z. Wang, Y. Li, X. Cai, D. Chen, G. Xie, K. Liu, Y.-C. Wu, C.-C. Lo, A. Lien, Y. Cao, and S.-J. Su, Structure-performance investigation of thioxanthone derivatives for developing color tunable highly efficient thermally activated delayed fluorescence emitters, ACS Appl. Mater. Interfaces **8**, 8627 (2016).

[148] Y. Kitamoto, T. Namikawa, D. Ikemizu, Y. Miyata, T. Suzuki, H. Kita, T. Sato, and S. Oi, Light blue and green thermally activated delayed fluorescence from 10h-phenoxaborin-derivatives and their application to organic light-emitting diodes, J. Mater. Chem. C **3**, 9122 (2015).

[149] Y. Sagara, K. Shizu, H. Tanaka, H. Miyazaki, K. Goushi, H. Kaji, and C. Adachi, Highly efficient thermally activated delayed fluorescence emitters with a small singlet-triplet energy gap and large oscillator strength, Chem. Lett. **44**, 360 (2015).

[150] K. Shizu, H. Tanaka, M. Uejima, T. Sato, K. Tanaka, H. Kaji, and C. Adachi, Strategy for designing electron donors for thermally activated delayed fluorescence emitters, J. Phys. Chem. C **119**, 1291 (2015).

[151] J. Lee, K. Shizu, H. Tanaka, H. Nomura, T. Yasuda, and C. Adachi, Oxadiazole- and triazole-based highly-efficient thermally activated delayed fluorescence emitters for organic light-emitting diodes, J. Mater. Chem. C **1**, 4599 (2013).

[152] M. Inoue, T. Serevilius, H. Nakanotani, K. Yoshida, T. Matsushima, S. Jurslnas, and C. Adachi, Effect of reverse intersystem crossing rate to suppress efficiency roll-off in organic light-emitting diodes with thermally activated delayed fluorescence emitters, Chem. Phys. Lett. **644**, 62 (2016).

[153] W.-L. Tsai, M.-H. Huang, W.-K. Lee, Y.-J. Hsu, K.-C. Pan, Y.-H. Huang, H.-C. Ting, M. Sarma, Y.-Y. Ho, H.-C. Hu *et al.*, A versatile thermally activated delayed fluorescence emitter for both highly efficient doped and non-doped organic light emitting devices, Chem. Commun. **51**, 13662 (2015).

[154] J. Lee, K. Shizu, H. Tanaka, H. Nakanotani, T. Yasuda, H. Kaji, and C. Adachi, Controlled emission colors and singlet-triplet energy gaps of dihydrophenazine-based thermally activated delayed fluorescence emitters, J. Mater. Chem. C **3**, 2175 (2015).

[155] Q. Zhang, J. Li, K. Shizu, S. Huang, S. Hirata, H. Miyazaki, and C. Adachi, Design of efficient thermally activated delayed fluorescence materials for pure blue organic light emitting diodes, J. Am. Chem. Soc. **134**, 14706 (2012).

[156] K. Bhattacharyya, Can TDDFT render the electronic excited states ordering of Azine derivative? A closer investigation with DLPNO-STEOM-CCSD, Chem. Phys. Lett. **779**, 138827 (2021).

[157] D. Mester and M. Kállay, A simple range-separated double-hybrid density functional theory for excited states, J. Chem. Theory Comput. **17**, 927 (2021).

[158] P. Pander, A. Swist, R. Motyka, J. Soloducho, F. B. Dias, and P. Data, Thermally activated delayed fluorescence with a narrow emission spectrum and organic room temperature phosphorescence by controlling spin-orbit coupling and phosphorescence lifetime of metal-free organic molecules, J. Mater. Chem. C **6**, 5434 (2018).

[159] T. J. Penfold, F. B. Dias, and A. P. Monkman, The theory of thermally activated delayed fluorescence for organic light emitting diodes, Chem. Commun. **54**, 3926 (2018).

[160] J. S. Ward, R. S. Nobuyasu, A. S. Batsanov, P. Data, A. P. Monkman, F. B. Dias, and M. R. Bryce, The interplay of thermally activated delayed fluorescence (TADF) and room temperature organic phosphorescence in sterically-constrained donor-acceptor charge-transfer molecules, Chem. Commun. **52**, 2612 (2016).

[161] J. Gibson, A. P. Monkman, and T. J. Penfold, The importance of vibronic coupling for efficient reverse intersystem crossing in thermally activated delayed fluorescence molecules, Chem. Phys. Chem. **17**, 2956 (2016).

[162] M. K. Etherington, J. Gibson, H. F. Higginbotham, T. J. Penfold, and A. P. Monkman, Revealing the spin-vibronic coupling mechanism of thermally activated delayed fluorescence, Nat. Commun. **7**, 13680 (2016).

[163] T. Northey, J. Stacey, and T. J. Penfold, The role of solid state solvation on the charge transfer state of a thermally activated delayed fluorescence emitter, J. Mater. Chem. C **5**, 11001 (2017).

[164] R. Ishimatsu, S. Matsunami, K. Shizu, C. Adachi, K. Nakano, and T. Imato, Solvent effect on thermally activated delayed fluorescence by 1,2,3,5-tetrakis(carbazol-9-yl)-4,6-dicyanobenzene, J. Phys. Chem. A **117**, 5607 (2013).